F., Mattei, M., Javadi, H. R., & Montemagni, C. (2021). Cenozoic dextral shearing along the Arusan sector of the Great Kavir–Doruneh Fault System (Central Iran). *Tectonics, 40*, e2021TC006766. https://doi.org/10.1029/2021TC006766

Cenozoic dextral shearing along the Arusan sector of the Great Kavir – Doruneh Fault System (Central Iran)

Andrea Zanchi[1], Stefano Zanchetta[1,*], Fabrizio Berra[2], Massimo Mattei[3], Hamid Reza Javadi[4] and Chiara Montemagni[1]

1: Dipartimento di Scienze dell'Ambiente e della Terra, Università degli Studi di Milano – Bicocca, Milano, Italy

2: Dipartimento di Scienze della Terra "Ardito Desio", Università degli Studi di Milano, Milano, Italy

3: Dipartimento di Scienze, Università Roma TRE, Roma, Italy

4: Geological Survey of Iran, Tehran, Iran

* corresponding author: stefano.zanchetta@unimib.it

A.Z.: 0000-0001-7190-6131

S.Z.: 0000-0001-7690-969X

F.B.: 0000-0002-4354-1806

M.M: 0000-0001-7800-8764

H.R.J.: 0000-0002-2660-6292

C.M.: 0000-0002-2850-9744

Key-words: intracontinental faults, Central Iran, wrench tectonics, transpression, Great Kavir Doruneh Fault System, paleostress

Abstract

The structural analysis of large intracontinental wrench faults is fundamental for deciphering the longterm evolution of continental crust in complex areas in terms of their geodynamic evolution and largescale crustal block displacements. In this contribution, we demonstrate a pre-Miocene dextral activity of the present-day left-lateral Great Kavir - Doruneh Fault System (GKDFS, Central Iran), one of the major intracontinental active strike -slip faults extending from the Afghan border to the Nain region between Central Iran and the Sanandaj-Sirjan Zone. We document important dextral shearing recorded a long a segment of the GKDFS, the Arusan Fault System (AFS), located east of Jandaq, close to the present-day active trace of the GKDFS. The AFS include several ENE-WSW striking strands exposed for a length of more than 50 km, which couple pre-Cretaceous ophiolites and metamorphic basement units with the Cretaceous succession of the Khur basin. The fault shows transpressional structures consistent with a dextral shear including thrusts and *en échelon* folds affecting the Cretaceous carbonate units. Paleostress reconstruction based on mesoscopic fault analysis and related folds geometry allowed to establish vorticity parameters indicating that deformation occurred close to a total simple shear regime with a calculated Wk between 0.9 and 1. The enormous Meso-Cenozoic dextral displacements occurred along the AFS and along the entire GKDFS are attested by the up to several hundreds of kilometers offset of the Paleotethys suture zone, from NE Iran to the western border of Central Iran.

1 Introduction

Strong deformation of continental crust along major wrench faults, resulting from large rotations of crustal blocks along vertical axes, was firstly suggested 50 years ago by Freund (1970) along the Dead Sea Transform. This phenomenon was later documented all over the world (e.g. Ron et al., 1984; Sonder et al., 1994; Storti et al., 2003; Walker & Jackson, 2004; Onderdonk, 2005; Mattei et al., 2015). Wrench tectonics is often responsible for large-scale (several hundreds to thousands of kilometers) displacements of previously continuous geological structures, such as orogens and major suture zones (Storetvedt 1974, 1987; Tapponnier et al., 1990). The Permian dextral mega-shear transforming Pangea -A to Pangea-B (Muttoni et al., 2009; Kent & Muttoni, 2020) and the displacement along the San Andrea Fault of the Baja California Peninsula (e.g. Mount & Suppe, 1987) are just some of the many examples of the role played by wrench tectonics in the evolution of continental crust.

One of the most fascinating and still unsolved problem of the geodynamic evolution of Iran is the enigma of block rotations within the internal portion of Central Iran (Figure 1). Starting from the first ideas of Davoudzadeh & Schmidt (1981) and Soffel et al. (1996), who have suggested a total

counterclockwise rotation of 135° of a large part of Central Iran with respect to stable Eurasia since the Triassic, recent works (Mattei et al., 2012, 2015, 2020) confirm that at least some blocks forming the Central Iran area may have rotated counterclockwise up to 80°-90° since the Jurassic. Evidence of this large-scale block rotations are also based on the displacement of the Paleotethys suture zone in NE Iran. Tectonic units related to the closure of the Paleotethys ocean were displaced from the Mashhad -Torbat Jam area south-westward to the north-western corner of Central Iran (Bagheri & Stampli, 2008; Zanchi et al., 2009b; 2015; Zanchetta et al., 2013; Berra et al., 2017; Balini et al., 2019) following the trace of the present-day Great Kavir – Doruneh Fault System (GKDFS). The idea of large-scale block rotations within Iran was also proposed by Alavi et al. (1997) and more recently by several authors (Balini et al., 2009, 2019; Zanchi et al., 2009b) to explain similarities between the Aghdarband Triassic succession of NE Iran and the Triassic of Nakhlak, which is located just north of Anarak in Central Iran (Figure 2).

Pirnia et al. (2020) argue about large crustal -scale rotations properly suggesting that the ophiolites of Sabzevar and Nain Baft, now located about 400 km from each other, were once part of a unique complex, which was possibly displaced along a precursor of the present-day GKDFS during the Cenozoic. Despite its present-day left–lateral motion, well documented by active tectonics and structural studies (Shabanian et al. 2009; Farbod et al., 2011; Bagheri et al., 2017), the idea that a large dextral displacement could have occurred along the GKDFS fits well also in paleogeographic reconstructions related to the Aptian time interval (Barrier & Vrielynk, 2008). These authors suggest, in fact, in their maps a dextral motion for the Great Kavir Fault, followed by a Late Cretaceous shift to left-lateral motion. Dextral shearing was also recognized in the central part of the GKDFS, where Tadayon et al. (2017, 2019) document dextral transpression during the early Cenozoic along the Taknar fault system, an important strand of the main fault. A shift from a long lasting right-lateral shearing to a post-Miocene active left-lateral motion was recently documented (Javadi et al., 2013, 2015). The accommodated left-lateral displacement is supposed to be of a few kilometers, with less than one kilometer during the Quaternary (Farbod et al., 2011, 2016).

In this paper, we present new original data on the post-Cretaceous right-lateral activity of an important ENE -WSW dextral shear zone, here named the Arusan Fault System (AFS), related to the western portion of the GKDFS. The AFS extends east of the town of Jandaq, a few kilometers to the south of the trace of the present day Great Kavir Fault which represents the western segment of the entire GKDFS. Several tectonic slices of ophiolitic units, the Jandaq ophiolites, are entrapped along the AFS, which also represent the northern boundary of the Cretaceous Khur platform, consisting of a carbonate-dominated succession. These features suggest that the AFS was a major fauls, separating the northern portion of Central Iran from the Yazd Block. We integrate field-based structural analyses with new stratig raphic reconstruction and mapping of the Cretaceous units, which provide a firm

evidence of Cenozoic dextral shearing along the precursors of the present-day GKDFS, adding new constraints on the evolution of Central Iran. Combining our new data with previous structural information, we propose a model in which the occurrence of dismembered fragments of the Paleotethys suture originally located in NE Iran and now exposed along the NW border of Central Iran is consistent with a large -scale dextral displacement occurred along an intracontinental fault, the AFS, representing a portion of its western sector.

2 Geological setting

2.1 Tectonic setting of Central Iran and surrounding area along the GKFDS

The GKDFS extends more than 700 kilometers from the border in NE Iran with Afghanistan running across the Iranian Plateau up to Nain (Figure 1a-b). This fault system, which shows an arcuate shape roughly trending E-W delimits the internal part of Central Iran, which is generally referred as the Central-Eastern Iran Microplate (CEIM). The CEIM is a very complex and still poorly known area, due to the occurrence of enormous sand deserts covering large part of the region. The CEIM is entirely surrounded by an Upper Cretaceous ophiolitic "ring", often known as the "coloured mélange" which delimits its most internal part. The ophiolitic ring includes different suture zones, from the Sistan to the East separating the CEIM from the Helmand and Farah blocks of Afghanistan to the Sabzevar ophiolites, which were deformed and emplaced between the end of the Cretaceous and the beginning of the Cenozoic, both showing HP metamorphism (Rossetti et al., 2015; Jentzer et al., 2020). A possible connection between the Sabzevar and the Nain ophiolites bordering the NW corner of the CEIM, both representing the remnants of Neotethys Cretaceous back-arcs, has been recently suggested by Pirn ia et al. (2020) based on compositional and geochemical affinities between the two suites. The CEIM consists of three major blocks, the Yazd, Tabas and Lut blocks separated by N-S trending active dextral faults, accommodating active deformation (Figure 1a). These blocks were part of the stable northern margin of Gondwana during most of the Paleozoic, as suggested by the affinity of their thick Paleozoic successions, which closely resemble the units exposed in the Alborz. A Precambrian metamorphic basement of Gondwanan affinity intruded by Cadomian granitoids is also common to the three blocks. During the Mesozoic, after the Cimmerian collision, they were covered by epicontinental seas taking to the deposition of thick carbonate and terrigenous successions (Wilmsen e al., 2015; 2018; 2020) followed by widespread Eocene volcanic activity and a shallow marine to continental succession of Oligocene to Miocene age. Terrigenous continental deposits characterize the post-Miocene sedimentation in the whole area.

In spite of these features, pointing to a general stability of the whole Central Iran, late Paleozoic to Triassic active margin units occur south of the GKDFS between Anarak and Jandaq. These units

show marked similarities with the complexes which mark the Paleotethys suture in NE Iran along the southern margin of the Turan plate, (Bagheri & Stampfli, 2008, Zanchi et al., 2009b, 2015; Zanchetta et al., 2013, 2018). Similar units occur also in the internal part of the CEIM in the Posht-e-Badam area along one of the major dextral faults separating the Yazd from the Tabas block (Bagheri & Stampfli, 2008; Kargaranbafgi et al., 2011).

2.2 Geological setting of the Arusan area along the Arusan Fault System (AFS)

The analysed structures (Figures 1 and 2) are exposed 50 kilometers to the east of Jandaq along the southern margin of the Great Kavir Desert, passing across the small oasis of Arusan, which gives the name to this fault system. The AFS consists of several ENE-WSW dextral strike-slip faults which crop out a few kilometers to the south of the active left-lateral Great Kavir Fault. The AFS is continuously exposed for more than 50 kilometers between Mesr and Airekan, flanking the Kuh-eKalateh ridge (Figure 3).

The oldest rocks in the area belong to a polymetamorphic basement (Early Jurassic) and to an ophiolitic unit, the Arusan ophiolitic mélange (Bagheri & Stampli, 2008; Torabi, 2009). Ophiolites form an imbricate system of thrust sheets with serpentinized peridotites, altered gabbros, metabasites and severely folded marble layers. The ophiolites are tectonically interleaved within the metamorphic basement unit including quartzites, metapelites, gneiss and amphibolites. Undeformed granitoids and pegmatite swarms are exposed along the AFS showing tectonic to intrusive contacts with the surrounding units. Late Jurassic K-Ar ages (158-147 Ma) were obtained on granites from this intrusive complex (Romanko et al., 19 79). These units are tectonically juxtaposed onto the Airekan granitic terrain which has given a Precambrian-early Cambrian U/Pb age obtained on a single zircon (549 ± 15 Ma; Bagheri and Stampfli, 2008) and alternatively a revised younger U/Pb Early Ordovician age (483 ± 2.9 Ma) following Shirdashtzadeh et al. (2018). The crystalline basement is discontinuously covered by the Chah Palang Fm., consisting of sandstones and conglomerates derived from the erosion of the underlying units. This unit, deposited between the Late Jurassic and the Early Cretaceous (Wilmsen et al., 2015), forms the base of the "mid" to Upper Cretaceous succession of the Khur Basin (Wilmsen et al., 2015) deposited to the south of the study area, which is part of the Yazd block of Central Iran.

3. Cretaceous stratigraphy of the Khur basin (Arusan area)

A deep revision of the local stratigraphic features of the Cretaceous succession of the Arusan area was needed as they differ from those of the central part of the Khur Basin (Wilmsen et al., 2015),

which represents our frame of reference. Sstratigraphic logs measured in the studied area are reported in Figure 4.

In the Arusan area, the crystalline basement is covered by the siliciclastic deposits of the Chah Palang Fm., discontinuously present at the base of the overlying Cretaceous carbonate succession (Fig ure 5a-b). The Chah Palang Fm. consists of conglomerates and sandstones, with clasts deriving from the underlying basement. The upper part of the unit is finer and richer in quartz grains, documenting a gradual increase in maturity. This siliciclastic unit likely filled depressions in the basement, smoothing the previous topography before the marine transgression marking the rapid and widespread deposition of Cretaceous carbonates in Central Iran. The thickness of the unit is extremely variable, from absent or reduced to a few centimetres sandstones and fine-grained conglomerates to more than 200 m. The unit is conformably covered by the Shah Kuh Fm. (Figure 4, Figure 5b), consisting of bioclastic limestone rich in orbitolinids and, locally, rudists, non-conformably laying on basement units. This unit is extremely continuous and characterized by a typical reddish alteration colour, with a thickness ranging from 80 up to 145 m. Locally, the upper part is faintly bedded, marked by hybrid limestones containing well-rounded quartz grains up to 1-2 cm in size, associated with marls and marly limestones, rich in orbitolinids and large bivalves. It is covered, with an erosional base, by red conglomerates with carbonate and basement clasts, passing laterally to sandstones and hybrid limestones, from about 50 to 90 m thick (Figure 5a). Due to its lateral and vertical variability, this interval cannot be easily referred to the Bazyab and Debarsu fms. of the Khur Basin. This unit is thinner with respect to the succession to the south (Wilmsen et al., 2015), and characterized by a coarser grain size, suggesting deposition close to the border of the basin.

The massive carbonates of the Haftoman Fm. follow up-section (Figure 4, Figures 5a and5b). They are made of siliciclastic limestones with quartz pebbles at the base. They usually display a light grey color and are purely carbonate in the upper part, where rudists are abundant. The unit is from 50 to about 85 m thick. The top of the Haftoman Fm. records a rapid drowning, with deposition of alternating limestones and marls, locally glauconitic. The succession above the Haftoman Fm. corresponds, for stratigraphic position, to the Farokhi Fm. of the Khur basin (Wilmsen et al., 2015). In the Arusan area, above a transitional unit with 80 m of well-bedded limestones, about 50 m of marls occur with intercalations of limestone beds and lenses, rich in orbitolinids and bivalves. These are covered by ca. 100 m of cherty limestones. A second marly horizon (about 50 m) with abundant zoophycos, with thin intercalations of bioclastic and cherty limestone containing glaucony follows and is covered by cherty limestones that likely contain the Cretaceous -Paleocene boundary (Figure 5c). Typical facies of these units exposed around Arusan are shown in Figure 5 (d - j).

4. Structural analyses

4.1 Methods

In order to characterize the geological and especially structural setting of the area crossed by the Arusan Fault System, our field analyses resulted in a general map (Figure 3) and two detailed original maps (Fig ures 6 and 7). We integrated our field observation with the analysis of Aster colour composite images and Google Earth detailed imagery (11-11-2013 views). The color composite satellite images used for mapping, a geological structural map together with a KML file with the localization of measurement sites, a table with the values used for paleostress analysis and field images of fault planes with kinematic indicators are available in the public Mendely Database (Zanchetta et al., 2021).

The Arusan Fault System (AFS) consists of several dextral strike-slip fault strands running along the slopes of the Kuh-e-Kalateh (Figures 3, 6 and 7), tectonically coupling the Cretaceous successions with the metamorphic basement and ophiolites. Tectonic slices of Mesozoic pinkish granitoids are exposed along the main fault, which runs to the NE of Kuh-e-Kalateh, passing across the village of Arusan and south of Mohammad Abad reaching Airekan within the Great Kavir desert (Figures 3 and 6). The fault trace can be followed from satellite images and available maps for more than 50 kilometers. Another important branch of the AFS, occurs west of Arusan, bordering the nameless reliefs (1435 m a.s.l.) exposing the Cretaceous cover; this branch of the fault system joins the main fault just west of Arusan with an overall lateral extension of about 15 kilometers (Figure 3).

Dextral faults with a comparable multi -kilometer linear extension also occur along the SE slopes of the Kuh-e-Kalateh close to the Naqi Spring (Figure 3), uplifting the metamorphic basement and the Chah Palang Fm. forming in-line anticlines within the Cretaceous carbonates.

We performed mesoscopic structural analyses in about 40 measurement stations located along the main tectonic structures. We measured several hundreds of fault planes with their slickensides, establishing the relative sense of motion through kinematic indicators as growth fibres, Riedel fractures, SC cleavage, etc. (Petit & Barquins, 1998). Folds and cleavages were also analysed in order to analytically evaluate their cylindricity and determine β fold axes.

4.2 The eastern branch of the Arusan Fault System (E-AFS)

This segment of the AFS is clearly visible on Google Earth satellite images (Figure 6), juxtaposing a thick sandstone succession of the Chah Palang Fm. to the Arusan ophiolites and metamorphic basement. Elongated horses of Mesozoic granites extending for several kilometers

occur along the fault, which shows a persistent vertical downthrown of at least some hundred meters relative to the SE block.

In the southern portion of the investigated segment (stop I14 -22: Figure 3), ENE-WSW to NE-SW dextral faults are associated to conjugate NW-SE left lateral faults and other secondary fractures affecting massive pinkish granitoids (I14-22); in a few stops the main right-lateral fault set is displaced by later normal faults showing throws up to a few meters (I17-5, I17-6).

We performed detailed analyses especially to the south of Arusan, mapping the area in order to extend our observations to the macroscale (Figure 6), based on new data on the stratigraphic setting. Here we observed a complex association of strike-slip, oblique-reverse and normal faults related to a large dextral fault zone with a maximum thickness ranging between 100 and 150 m. The AFS displays here an anastomosed pattern (stops I14-6, I15-1, 15-2, 15-21, 15-22, 17-1), characterized by dextral motions on subvertical fault planes with both slight normal and reverse oblique components (pitch up to 35°) and subordinate reverse oblique motions forming a flower structure (Figure 8, section A-A'). The fault zone consists of several vertical horses tens of meters thick, including the quartzite basement, large portions of the Mesozoic granitoids, and the Chah Palang Fm., which are tectonically coupled with the carbonates of the Shah Kuh Fm. along a dextral reverse SE-dipping shear zone showing an up to five meters thick fault core with coarse-grained foliated cataclasites. A cleavage related to dextral SC shear bands formed all along the fault zone (Zanchetta et al., 2021).

The high-angle oblique fault zone passes southward to a thrust plane (Figure 8, section B-B') stacking the quartzite basement onto the upper part of the Shah Kuh Fm. (Figure 9), thus causing a tectonic repetition of the lower part of the Cretaceous succession (Figure 8, section B-B'). The contact between the basement and the Shah Kuh Fm. in the thrust hanging wall is also faulted showing thin tectonic slices of the Chah Palang Fm., which has been tectonically elided. The hanging wall of the thrust consists of a reduced succession, in which the carbonates of the Shah Kuh directly grade to bioclastic massive limestone of the Haftoman Fm. with a few intercalations of hybrid calcarenite and calcirudite beds containing siliceous clasts (Figure 10a). The basement horse thins out southward, its displacement being accommodated by a thrust plane propagated within the Shah Kuh Fm. of the lower unit forming an additional horse (Figure 8, section C-C'). Both thrust planes stop against a transversal NW-SE left lateral tear fault. SW of this fault the thrust surface is shifted into an upper structural position along the marly layers which separate the Shah Kuh from the Haftoman Fm. (Figure 8, section D-D'), dying out progressively to the SW along the north side of the Kalateh ridge. Regularly spaced left -lateral faults with a horizontal separation of a few hundred meters and normal faults with a WNW-ESE strike (I15-24, I15-25), geometrically consistent with a dextral shear along the master fault (Figure 9b), displace the Cretaceous units in the hanging-wall, sharply stopping

against the master fault, which crosscuts all these secondary structures (Figure 8, section B-B'). Around the village of Arusan, the fault shows dextral strike-slip kinematic indicators (stop I14-6) along the contact between reddish granitoids and the Farokhi Fm. Altered pseudotachylyte veins occur just to the south of Arusan in the granites along NE-SW dextral faults related to the main system (stop I14-5). The occurrence of cohesive cataclasites, suggest that deformation started at some kilometers of depth (Zanchetta et al., 2021).

The eastern portion of the fault is poorly exposed south of the oasis of Mohammad Abad (Figures 2 and 3), where the metamorphic basement and the Mesozoic granitoids are tectonically coupled with the Chah Palang Fm. The contact is covered with recent deposits and we observed secondary faults trending between ENE -WSW to ESE-WNW with a dextral displacement based on *en échelon* veins (stops I15-31, I15-32; Supplementary Figure 1). In this area, as well, part of the contact between the Chah Palang Fm. and the overlying carbonates of the Shah Kuh Fm. consists of a low-angle fault with a reverse slip based on cleavage orientation (stop I15-33, Zanchetta et al., 2021).

4.3 The western branch of the Arusan Fault System (W-AFS)

Another important fault zone develops to the WSW of Arusan along the southern contact between the crystalline basement and the Cretaceous cover (Figures 3 and 7). The fault zone, which is markedly oblique to the structures of the basement, joins the main branch of the AFS at Arusan, following an ENE-WSW strike. The fault zone is delimited by two parallel faults dipping to the north (Figure 7). The southern one follows the contacts between the cover and the basement, whereas the northern one propagated inside the cover, separating the high strain deformation zone from a poorly deformed block to the north, which shows a continuous Cretaceous stratigraphic succession directly covering the Jandaq metamorphic basement. The fault system produces a lens-shaped deformation zone large about 200-300 meters with NE-SW trending en échelon folds (Figure 7; stops I15-10, I1518, I 15-29-35-36), isolated folds trending NE-SW to NNE-SSW (stops I15-13, I15-37) and small thrusts forming two small klippen in the Shah Kuh and Haftoman fms., with disharmonic folds below the thrust planes (Figure 10c,e).

In spite of the marked transpressional character of the fault zone indicated by the occurrence of fold and thrust structures, mesoscopic fault populations mainly record dextral motions with a small oblique normal component (stops I15-9, I15-11, 15-15 15-37, Figure 7), or both oblique normal and reverse moti ons (stops I15-12, I15/16/17, Figure 7). This kinematic features result in the lowering of the Cretaceous succession of the hanging wall with respect to the basement.

Variably oriented normal faults (stops I14-30, I15-19/20, I15-26/27, I15-35/36/37; Figure 7) are often superposed on the strike-slip system all over the area. ESE-WSW normal faults with displacements

limited to a few meters, geometrically consistent with a dextral shear, occur also in the hanging wall, the largest one varying progressively fr om west to east into a dextral fault (stop I15-37, Figure 7).

4.4 The Naqi Spring Fault

The SE strand of the AFS runs along the eastern slope of the Kalateh Ridge in the area of the Naqi oasis (Figure 3). Here the metamorphic basement and the Chah Palang Fm. are uplifted among the carbonates of the Shah Kuh and Haftoman fms. along NE-SW trending strike-slip faults. The Chah Palang Fm. is severely deformed (I15-7, Figure 3 and Supplementary Figure 1) with SE-verging asymmetric inclined folds (Figure 10d). South of Naqi, similarly to what described along the eastern segment of the AFS, a small klippe of highly fractured and dismembered Shah Kuh Fm. overlies the Chah Palang deformed sandstones in the middle of the valley forming an isolated relief (Figure 10d). The klippe is likely related to a detachment developed between layers with a different rheology given by the underlying folded thin-bedded sandstones and the overlying massive carbonates. Strike-slip faults follow the marly layers of the Farokhi Fm. as suggested by their progressive closure (Figure 5c). In the southern portion of the investigated segment (stop I14-22: Figure 3), ENE-WSW to NE-SW dextral faults are associated to conjugate NW-SE left lateral faults and other secondary fractures affecting massive pinkish granitoids (I14-22); in a few stops the main right-lateral fault set is displaced by later normal faults showing throws up to a few meters (I17 -5, I17-6).

5. Paleostress versus strain analyses and structural evolution

5.1 Methods

Selected fault populations were analysed in terms of paleostress determinations (Angelier, 1990; Delvaux & Sperner, 2003 and ref. therein). This technique allows to establish the compatibility among faults showing complex geometry and kinematics, as well as to distinguish fault populations related to different tectonic stages based on rational numerical criteria. Paleostress reconstruction has been applied in several areas of Iran helping to define its complex evolution (Navabpour et al., 2007; Javadi et al., 2013, 2015; Jentzer et al., 2017, Zanchi et al., 2006; 2009a; 2016), ensuring significant results in areas characterized by complex strain patterns related to transpressional and contractional regimes. Results are especially relevant when measured faults are related to small and homogeneous displacements showing a pure shear coaxial deformation. We refer to Angelier (1984, 1990, 2002) and to Delvaux and Sperner (2003) for theoretical principles of the method and adopted algorithms. Paleostress reconstruction was performed in eleven sites (Figures 11 and 12), in which a sufficient number of striated fault planes occurs. Results of inversion in terms of the obtained reduced stress

tensor are reported in Table 1. We also prepared rose and Frolich diagrams in Wintensor to synthetize the geometrical features of the measured faults.

We used fold data for strain analyses considering geometrical relationships between fault zones, cleavage and folds to determine vorticity parameters, which help to evaluate quantitatively the dominant tectonic regime along the studied strike-slip zones. Transtentional and transpressional shear zones are the result of a simultaneous combination of simple shear and pure shear (Fossen et al., 1994) and can be expressed by the dimensionless kinematic vorticity number Wk (Truesdell, 1953) for any kind of flow. Wk, defined as the relative rate of stretching to rotation (Fossen & Tykoff, 1998), varies between 0 for pure shear and 1 for simple shear (Means et al., 1980). Based on the orientation of the Instantaneous Stretching Axes (ISAs) with respect to the shear zone boundary indicated by the θ angle (Fossen et al., 1994), transtension ($\theta > 45°$) can be separated by transpression ($\theta < 45°$). In addition, Fossen and Tikoff (1993) defined two types of transtension and two types of transpression: wrench- (simple shear) dominated and pure-shear dominated.

After calculating paleostress axes, since as reported by Weijermars (1991), the ISAs can be linked under certain conditions to the principal stress axes, we measured the angle θ between the σ_3 (corresponding to the ISA_1) in the horizontal plane and the fault zone boundary (Figure 13a). As we have considered that strain increments were infinitesimal the maximum ISA (ISA_1) corresponds to the direction of minimum stress axis (σ_3). The relationships between the ISA_1 and the shear zone boundary are related to the kinematic vorticity number W_k (Figure 13; Fossen & Tikoff, 1993; Fossen et al., 1994; Fossen & Tykoff, 1998) by the equation $W_k=\cos(90°-2\theta)$, suggested in Fossen and Cavalcante (2017).

In transpressional and transtentional zones, linear as well as planar markers rotate during progressive deformation (Fossen et al., 1994) due to the contribution of pure and simple shear components. This applies both fo r pre-existing markers and for those that form during deformation. Such structures comprise, among others, also fold axes, which rotate depending on the W_k of deformation.

Therefore, using the software ArcGIS (esri©), we measured the angle between the trend of the fold axes and the shear zone boundary (Figure 13b) assuming that any rotational incremental strain occurred during deformation and that orientation of fold axes is parallel to ISA_1 (Fossen et al., 1994; Tadayon et al., 2019).

The results of fie ld-based geological observations, fault and fold analyses, paleostress inversion and strain analyses, were integrated to reconstruct the relative chronology among the studied structures. We suggest the occurrence of two main different deformation stages, which can be related to the Cenozoic evolution of this portion of Central Iran.

5.1 Stage 1: NW-verging thrust stacking

This event largely affects the crystalline basement of the area. The contacts among the Arusan ophiolites, the metamorphic basement and the Mesozoic granitoids generally consist of dip-slip SEdipping reverse and thrust faults forming a NW-verging thrust fan. Fault populations characteristic of this stage (Figure 11) are related to internal stacking among the serpentinite bodies of the Arusan ophiolites (Figure 10e) and the different units of the metamorphic basement. Faults inversion at stop I13-12 (Figure 11a), which is fully representative of this stage, shows a pure compression with a horizontal NW-SE σ_1 and a vertical σ_3. Fault planes are superposed on previous brittle-ductile shear zones with the same dip, dip-direction and kinematics, suggesting a continuous evolution from ductile to brittle conditions. This is suggested by a down-dip orientation of the stretching lineation on mylonites developed along these shear zones and by their top-to-NW shear sense (Figures 10e and 11b). Field relationships among fault population show that these thrust zones (Figure 11a-c) are crosscut by ENE-WSW dextral faults (Figure 11d), which are related to the successive deformation stage.

5.2 Stage 2: NE-SW dextral shearing

Most of the fault populations and folds measured within the Cretaceous units refer to this event, which corresponds to the activation of the Arusan Fault System with a dextral shear sense. This stage (Figures 11d and 12) is characterized by a predominance of NE-SW right-lateral fairly pure strikeslip faults often conjugate to NW-SE left-lateral strike-slip faults resulting in a horizontal σ_1 trending from WNW-ESE to a dominant NW-SE trend, a horizontal σ_3 and consequently in a vertical σ_2. At stop I15-15, along the western termination of the western segment of the AFS, we observe a vertical σ_1 and a horizontal NE -SW trending σ_3 possibly due to stress axes permutation between σ_1 and σ_2 along this part of the structure, which shows a significant normal throw of the hanging-wall. Relevant paleostress determinations were obtained for the faults measured along the two main segments of the AFS and are broadly coherent all across the study area. The one exception is given by the small thrust faults measured close to the Naqi Spring (stop I15-7; Supplementary Figure 1), which suggest an E-W pure compression, probably related to local strain partitioning or variations in the paleostress orientation.

Complex relationships among the strike -slip Arusan Eastern Fault and thrust faults occur SW of Arusan, where the basement and the base of the Cretaceous cover are thrusted on the lower part of the Cretaceous succession, forming a double to triple tectonic repetition of the Shah Kuh Fm. (Figure 9). As observed in the field, the main thrust surface is crosscut by both dextral and left lateral faults. This suggests that it can be related to the NW-SE compression observed within the basement, or,

alternat ively, to the first stages of the growth of the AFS, forming a restraining bend, which was later crosscut by the high angle NE-SW dextral faults. A transpressional character of the deformation is, in fact, evident along both segments of the AFS. The western segment shows as well a marked transpression in its central part, which is characterized by *en échelon* fold trains and small thrusts. Normal faults with ESE-WNW also occur in the hanging wall of both faults suggesting a complex triclinic strain pattern (Diaz-Azpiroz et al., 2014). We also observed other small normal faults with variable orientations, which can be related to a younger stage.

Geometrical relationships between the trace of shear zone boundaries and the orientation of σ_3 obtained with paleostress analyses allowed us to determine vorticity parameters (Figure 13): our data suggest a wrench dominated regime (Figure 13a; Fossen & Tikoff, 1993; Fossen et al., 1994) for both the Arusan Western Fault (Wk = 0.95-1.0) and the Arusan Eastern Fault (Wk = 0.90-1.0) shear zone (Figure 13a).

For the Arusan Western Fault shear zone, in which isolated and *en échelon* folds occur, we obtained a pure shear dominated transpression (Figure 13b), suggesting that the first stages of deformation were accommodated by folding. After this first folding stage, deformation shifted along newly formed faults, as suggested by paleostress reconstruction.

6. Discussion

The idea that the GKDFS might be a major structure inherited from the Mesozoic evolution of Central Iran and related to the opening of the Sabzevar Ocean was firstly suggested based on paleogeographic reconstructions (Barrier and Vrielynk, 2008; Morin et al., 2018). These authors proposed an older dextral shearing related to the opening of the Sistan-Sabzevar Ocean followed by inversion of the shear sense at the end of the Cretaceous that led to the closure of the basin.

Structural observations from the eastern (Javadi et al., 2013), central (Javadi et al., 2013; Tadayon et al., 2017) and westernmost (Javadi et al., 2015) sector of the fault system confirmed an important phase of dextral transpression preceding the post- Miocene left-lateral motion. This older phase has been mainly documented along secondary faults (Javadi et al., 2013, 2015; Tadayon et al., 2017) that were part of the GKDFS and are now located both to the north and south of the present-day main fault trace. That the AFS was part of the GKDFS is testified by the fact that it represents the northern boundary of the mid to Upper Cretaceous succession of the Khur basin (Wilmsen et al., 2015) belonging to the Yadz block of the CEIM. The stratigraphic succession cropping out to the north of the AFS displays a different paleogeographic affinity (Barrier and Vrielynck, 2008; Wilmsen et al., 2015), indicating that the AFS is a major tectonic discontinuity separating continental blocks that experienced distinct tectonic and stratigraphic evolution in pre-Cenozoic times.

The AFS, located in the central sector of GKDFS, has never been studied in detail and the occurrence of a pre-late Miocene dextral transpression all along the GKDFS was until now not adequately supported. A dextral motion experienced by the whole GKDFS is mandatory in order to support the idea that CEIM blocks experienced a counter clockwise rotation of ca. 35° during the Cenozoic as suggested by paleomagnetic data (Mattei et al., 2015).

6.1 Comparison of the AFS with the evolution of the GKDFS

Evidence of an early activity of the GKDFS accommodating NW-SE directed compression was reported in several areas along the fault trace and adjacent areas. The thrust fan dismembering the Anarak Metamorphic Complex (Bagheri & Stampfli, 2008, Zanchi et al., 2009b, 2015), stacking the Carboniferous accretionary wedge within the Cenozoic succession, was interpreted as an expression of the SW termination of the dextral fault zone (Javadi et al., 2015). In addition, the dextral transpressional structures north of Doruneh, related to *en échelon* folds and to the north of the Taknar Fault, were interpreted as a pre-Pliocene right-lateral imbricate fan (Javadi et al., 2013).

A multi-stage evolution of the GKDFS was documented also for its central segment (between Doruneh and Kashmar, Figure 1). Structural, stratigraphic and thermochronological data all point to a polyphase history of the fault (Tadayon et al., 2017, 2019). The provided tectono-stratigraphic evolution includes a first stage of thrust stacking of the ophiolitic units accompanied by the inversion of the Late Cretaceous normal faults bounding the Sabzevar oceanic basin under a NW-SE directed shortening. In this interpretation, shortening resumed at the end of the Eocene, following the same NW-SE direction of compression accompanied by E-W dextral shearing causing the activation of a dextral contractional stepover in the Taknar region, which was followed by a steady-state continuous growth of the structure (Tadayon et al., 2019). North of Kashmar, NE -SW oriented, NW-dipping dipslip thrust faults stacked the Permian and Cretaceous successions onto the Eocene and were crosscut by almost pure strike-slip E-W trending dextral faults (Tadayon et al., 2017).

The precursors of the GKDFS post-date subduction in the Sabzevar region, as testified by the age of magmatic rocks that intruded blueschists-bearing metamorphic units related to the Sabzevar subduction accretionary wedge (Rossetti et al., 2015).

A change in the stress regime from a NW -SE to a N-S direction of compression occurred in both areas around the Miocene-Pliocene transition, causing a dramatic change in fault kinematics, with the shift of the GKDFS to a left-lateral transpressional system (Tadayon et al., 2017, 2019).

The AFS, here analysed for the first time, displays an evolution that is broadly similar to the one of the GKDFS. A first stage of NW-SE directed compression, activating NW-verging thrust system within the Jandaq metamorphic basement and ophiolites and possibly in the Cretaceous cover, was

followed by important dextral shearing along ENE-WSW and NE-SW strike-slip faults associated to the formation of major transpressional structures and minor transtensional faults suggesting a complex triclinic shearing. These structures of the second stage crosscut the previously formed thrust sheets (Figure 9). The formation of thrust stacks with the same attitude within the Cretaceous cover suggests a Cenozoic deformation age, as the deformed Upper Cretaceous succession extends conformably at least to the Paleocene. More accurate time constraints on the age of this deformation phase are provided by Javadi et al. (2013) and by Tadayon et al. (2019) along other sectors of the GKDFS. Dextral faulting under a NW-SE compression follows in time thrust stacking, and was active up to the middle Miocene (Javadi et al., 2013) or up to the Tortonian (Javadi et al., 2015), from the age of the youngest rocks deformed by dextral faults along the western segment of the GKDFS. Considering the thrust system displacing the upper Paleozoic Anarak Metamorphic Complex related to the western termination of the right-lateral GKDFS, deformation could be constrained to the latest Miocene (Javadi et al., 2015). Farbod et al. (2011) also proposed a NW-SE compression on the basis of paleostress analyses along the central segment of the GKDFS given by E-W dextral strike-slip faults measured in pre-Pliocene rocks, whereas recent Pliocene to Quaternary faults are always consistent with a NE-SW contraction and a left-lateral shear sense of the fault.

Available data indicates that dextral shearing in response of a NW-SE directed shortening is not a local feature strictly related to the GKDFS, but it is documented in other adjacent areas, like the Alborz, during the late Cenozoic (Allen et al., 2003, Guest et al., 2006, Zanchi et al., 2006). The Alborz orogenic belt acted as a distributed accommodation zone of dextral shearing up to the Kopeh Dagh, before oroclinal bending occurred (Mattei et al., 2017), as well as along secondary branches of GKDFS (Nozaem et al., 2013).

A similar evolution of the regional stress regime is reported also in the Sistan belt of East Iran, with a Miocene E-W compression followed by a CCW re-orientation to NE-SW and NNE-SSW compressions during Pliocene and Quaternary, attesting full mechanical coupling of the Sistan Belt with the Zagros region only after the Miocene (Jentzer et al., 2017).

This is a major critical point, as the studied area together with the Taknar (just NW of Kashmar, Figure 1) and surrounding regions display a NW-SE compression during the early Cenozoic, which is at odds with the paleostress pattern reconstructed along the Zagros belt during pre -Pliocene times through fault analyses (Navabpour et al., 2007). This suggests scarce coupling with the Zagros to the west, whereas more similarities are evident with the whole region east of the Sanandaj-Sirjan. We speculate that this particular stress and strain patterns can result from an independent stress field induced by CCW rotations of rigid blocks to the south of the GKDFS, which was probably in continuity with the Herat dextral Fault in Afghanistan during a large part of the Cenozoic. Important block rotations occurring between the closing Sistan Belt, subjected to an E-W compression and the Makran region under a continuous NNE-SSW shortening during the Cenozoic (Dolati and Burg, 2013) was possibly induced by the post-Eocene indentation of India with the Eurasian margin,

causing the extrusion of crustal-scale blocks also along its western margin. A similar scenario was also suggested in Bagheri (2021), who considered the evolution of the Sistan Belt as the result of large-scale oroclinal bending around a vertical axis following the westward tectonic escape of the Afghan block prompted by the India-Eurasia collision. In this geodynamic framework, the CCW rotation of the Lut Block is a direct consequence of the oroclinal bending of the Sistan Belt.

On the other hand, Tadayon et al. (2019) find a good correspondence in time among the main stages of the evolution of the Zagros belt, the Arabia-Eurasia collision and the studied area of Central Iran.

6.2 The remnants of the Paleotethys suture zone along the GKDFS and adjoining

The remnants of the Paleotethys suture zone have been recognized in several areas of Iran, from Alborz, to NE Iran and Central Iran (Stocklin, 1974; Alavi, 1991; Ruttner et al., 1991; Ruttner 1993; Zanchetta et al., 2013; Moghadam et al., 2015; Sheikholeslami et al., 2019; Sheikholeslami & Koupeyma, 2012). In the Mashhad area of NE Iran the Paleotethys remnants consist of the ultramafics-bearing Binalood metamorphic complex (Sheikholeslami et al., 2019; Sheikholeslami & Khoupeyma, 2012), which have been related with a trench environment by Alavi (1991). Moving NE -ward, the mid Paleozoic orogenic complexes of Darreh Anjir (Zanchetta et al., 2013; Moghadam et al., 2015), the Permian turbiditic complex with carbonate olistoliths exposed between Mashhad and Torbat Jam (Zanchetta et al., 2013), together with the Triassic volcanoclastic succession of Aghdarband (Ruttner, 1991; Alavi et al., 1997; Balini et al., 2009; Zanchi et al., 2016; Balini et al., 2019) point to the existence of an active convergent margin from the Devonian up to the Middle Triassic. The Upper Triassic granitoids of Mashhad (Karimpour et al., 2010; Mirnejad et al., 2013) and Torbat Jam (Zanchetta et al., 2013) intruded the deformed units providing a minimum age for collision. The last significant tectonic event affecting the Paleotethys suture zone occurred during th e Early Jurassic (Sheikholeslami et al., 2019) with penetrative deformation and associated metamorphism up to amphibolite facies conditions (Sheikholeslami et al., 2019; Sheikholeslami & Khoupeyma, 2012).

Correlation among the described units of the Paleotethys suture of NE Iran and the dispersed crustal fragments exposed in the NW border of the CEIM is a major conundrum of the crustal scale geology of Iran. Systematic investigations of these blocks followed by regional scale correlations performed in recent years (Bagheri & Stampfli, 2008; Zanchi et al., 2009b; Balini et al., 2009; Zanchi et al., 2015; Berra et al., 2017; Zanchetta et al., 2018) suggest that the Paleothetys suture zone could have been displaced along the GKDFS for several hundreds of kilometers.

The oldest units recognized close to Jandaq occur in the Godar-e-Siah Complex, where a Devonian to Carboniferous succession described by Sharkowski et al. (1984) contains Carboniferous brachiopod faunas and foraminifera with a northern European affinity (Berra et al., 2017). The U-Pb zircon data obtained from granitoid boulders found in conglomerates exposed in the same area provided a Late Devonian to Mississippian age (Berra et al., 2017), testifying to the occurrence of an active magmatic arc during the Devonian and its subsequent deep erosion during the Paleozoic. The occurrence of an active margin during the Carboniferous within the CEIM is provided by the Carboniferous Anarak Metamorphic Complex (Bagheri & Stampli, 2008; Zanchi et al., 2015), located between Jandaq and the town of Anarak to the south, showing subduction-related HP-LT metamorphism and deformation during the Late Carboniferous (Zanchi et al., 2015; Zanchetta et al., 2018).

In addition, the Triassic volcanoclastic succession of Nakhlak (Figure 2), which contains deep-water sediments interlayered with volcanic arc products, ammonite faunas, undeformed granitic clasts and rock fragments derived from a metamorphic basement, has been correlated with the Aghdarband succession (Ruttner, 1991; Alavi et al., 1997, Balini et al., 2009; Zanchi et al., 2009b; Balini et al., 2019). The two areas are the only ones where a Lower to Middle Triassic deep water marine succession deposited in an active arc environment crops out. During the same time, in fact, the entire Iranian plate was covered by shallow sea carbonate platforms (Elika Fm.), pointing to a paleogeographical affinity of the two successions currently separated by more than 600 kilometers. The Posht-e-Badam Complex, located between the two dextral strike-slip Posht-e-Badam and Chapedony faults, gives additional evidence of a displaced fragment of the Paleotethys suture within the interior of the CEIM. Its present-day position has been interpreted as the result of large-scale CCW of the Yazd Block along dextral large-scale sub-circular shear zones juxtaposing this unit between the two Yazd and Tabas blocks (Bagheri & Stampli, 2008). The Posht-e-Badam Complex bears several similarities with the Anarak -Jandaq units (Davoudzadeh & Weber-Diefenbach, 1997), as it shows Carboniferous metamorphic ages and it was intruded by Upper Triassic granites and granodiorites (Ramezani & Tucker, 2003). Evidence of Cimmerian deformation and metamorphism in this area was recently confirmed by ^{40}Ar-^{39}Ar amphibole ages of ca. 220 Ma (Kargaranbafghi et al., 2012).

Pirnia et al. (2020) also proposed possible displacements of large blocks related to the CCW rotations of the CEIM, based on the strong similarities in composition and origin between the Sabzevar and the Nain-Ashin ophiolites, now lying more than 300 km apart (Figure 1a). According to these authors, both units derived from a suprasubduction volcanic arc setting, active during the Early Cretaceous along the northern margin of the CEIM. This margin was possibly in continuity with the northern

portion of the Sistan Ocean and they were displaced, together with their continental basement, along a dextral precursor of the GKDF during the Cenozoic. This new hypothesis is in contrast with previous interpretat ions correlating Nain and Baft ophiolites to the same origin in a back-arc position with respect to the Sanandaj-Sirjan Mesozoic active margin located to the SW of Central Iran (e.g. Hassanzadeh & Wernicke, 2016).

6.3 The CEIM blocks rotation and the GKDFS

The idea of a strong internal rotation of continental blocks forming the CEIM was born forty years ago (Davoudzadeh & Schmidt, 1981). It was supported by the first paleomagnetic data produced on this area by Soffel et al. (1996), suggesting a CCW rotation along vertical axes of the entire region up to 135°. Based on new paleomagnetic data from the Upper Jurassic of the Yazd, Tabas and Lut blocks, the amount of CCW rotations was evaluated between 45°(±11°) and 82°(±14°) with a mean value of 66° (±13°), whereas paleomagnetic directions from the Cretaceous of the Yazd and Tabas blocks show a smaller amount of CCW rotations comprised between 18° (±13°) and 47° (±13°), with a mean value of 34° (±15°)(Mattei et al., 2015). Paleogene paleomagnetic directions from the Yazd, Tabas and Lut blocks show CCW rotations ranging between 91° (±20°) and 20° (±9°), with a mean value of 43° (±14°) , whereas Miocene CCW paleomagnetic rotations in the Yazd and Tabas blocks are about 20° (±8°) (Mattei et al. 2012; 2020).

These data indicate that the CEIM was affected by two main stages of rotations (Figure 14). An older phase, which occurred during the Early Cretaceous with an amount of ~30° CCW, and a more recent phase, which accomplished an additional ~35° CCW, ~20° of which occurred in the last 10 Myr (Mattei et al., 2015).

The Early Cretaceous rotation is likely related to the evolution of the Sistan Ocean. The existence of an oceanic basin in the Sistan from the early Aptian to Albian, separating the Afghan from the Lut block, is proved by paleontological data (Babazadeh and de Waver, 2004) and geochronological data (Zarrinkoub et al., 2012). The oceanic basin likely reached a width of ca. 1000 km (Barrier and Vrielynk, 2008) and its closure started around the Late Cretaceous, as suggested by the age of blueschists and eclogites (Brocker et al., 2013; Jentzer et al., 2017; Bonnet et al., 2018) that testify to ongoing subduction. Paleogeographic reconstructions (Barrier and Vrielynk, 2008) suggest that the Sistan Ocean opened from south to north. We propose that the progressive opening promoted a westward motion of the Lut block that moved away from the Afghan block and contemporaneously rotated along the precursor of the GKDFS

Before rotations, the Lut, Tabas and Yadz blocks forming the CEIM were presumably oriented WSWESE with the Lut block facing southward the Neotethys, as proposed by Wilmsen at al. (2015).

A subsequent rotation stage occurred after the Oligocene producing a total CCW rotation of ~35°, with a mean-age rotation of ~20° during the last 10 Mys, following a long time lapse during which no rotations along vertical axes were recorded by CEIM continental blocks. According to Mattei et al. (2012, 2020), Cenozoic rotations accommodated NNE-SSW shortening related to the convergence between Arabia and Eurasia. In this framework, N-S trending dextral faults favoured CCW rotations of the single blocks forming the CEIM, whereas to the north of the Doruneh Fault, poor or no clockwise rotations occurred (Mattei et al., 2012; Walker & Jackson, 2004). It is important to stress that these large-scale paleomagnetic rotations are confined to the CEIM, as no such rotations were measured outside its borders, although post-Miocene oroclinal bending is responsible for the present curvature of the Alborz Mountains to the north, due to Arabia-Eurasia indentation in front of the rigid South Caspian Basin (Mattei et al., 2015, 2017, 2019).

This two stages rotation model (Figure 14) can explain the scenario of differential displacement of large crustal blocks within and around CEIM. The larger displacement shown by the upper Paleozoic to Triassic Paleotethys fragments with respect to the horizontal separation occurring between the Sabzevar and the Nain-Ashin arc-related "ophiolites" can be thus explained in terms of their different age of formation. The Paleotethys suture was affected by the maximum amount of CCW vertical axes rotations, which has been recorded at least from the Jurassic-Cretaceous boundary, contemporaneously with the opening of the Sabzevar and Sistan oceanic basin around the CEIM. Wrench tectonics accompanying the post-collisional stage of the Cimmerian orogeny (Zanchi et al., 2016) may have favoured additional displacements starting from the end of the Triassic. The second significant stage of CCW rotations occurred during the Cenozoic after a long time of null rotations and can be directly related with the dextral activity of the Doruneh Fault System and related structures as recognized by stru ctural analyses carried out all along the fault zone. According to this idea, Javadi et al. (2013) evaluated a Cenozoic displacement of about 280 kilometers along the GKDFS, which can help to restore the Nain-Ashin ophiolites to their original position closer to Sabzevar and to accomplish the entire rotations of the Paleotethys blocks up to the NW corner of the CEIM. The approximate curvilinear geometry of the GKDFS and of the other major faults responsible for the rotations of the Posht -e-Badam block are additional indications of the occurring rotation along a stable pivot point which can be located in the southern part of the CEIM with limited variations through time (Figure 14).

The CCW rotation of the CEIM crustal block could had been activated in response to the tectonic evolution of adjacent areas to the east, i.e. the Makran subduction zone characterized by a N-NESSW shortening (Dolati and Burg, 2013) and the evolution of the Sistan Belt, which was influenced by the westward escape of tectonic blocks due to the India-Eurasia indentation south of the prePliocene

GKFDS -Herat dextral system, rather than to the progressive building of the Zagros belt. This interpretation is consistent with the absence of rotation of the Sanandaj-Sirjan crustal block during the same time interval.

7. Conclusions

Integrated structural and stratigraphic analyses and detailed geological mapping of an ENE-WSW fault system of regional importance (the Arusan Fault System) in the NE sector of the CEIM, just south of the present-day active Great Kavir – Doruneh Fault, take to the following main results:

- The AFS, including two main fault strands (the western and eastern ones), shows dextral motion all along its development, accompanied by transtensional and transpressional structures. Based on crosscutting relationships, transpressional structures resulting in *en échelon* folds and thrusts formed along the western segment during dextral shear. The eastern segment shows relationships that are more complex, as thrust faults laterally pass to a dextral transpressional shear zone which crosscut NW-SE normal faults and NNE-SSW left-lateral strike-slip faults consistent with a dextral shear. Both segments of the AFS display similar kinematic and geological features. Both fault zones juxtapose strongly uplifted Mesozoic crystalline basement rocks including amphibolite facies metamorphic rocks and ophiolites to the Cretaceous carbonate succession, which is underlain by the Chah Palang ?Upper JurassicLower Cretaceous conglomerates directly resting on the basement.
- Two main tectonic stages could be recognized in the Arusan area: (i) an older one related to a NW-SE compression stacking the basement and the ophiolites in a NW-verging thrust fan; (ii) a younger event related to the development of ENE-WSW dextral strike-slip faults that crosscut and/or reactivate thrust faults related to the older event. Structures that could be correlated with the first event, on the base of their trend and kinematics, also affect the Cretaceous succession just south of Arusan, suggesting a post-Cretaceous, “mid” Cenozoic deformation age.

Paleostress analyses carried out in several sites along fault strike give homogeneous results, with the main horizontal stress axes σ1 and σ3 trending respectively NW-SE and NE-SW in a dominant transtensional regime.

The proposed structural reconstructions are consistent with the regional evolution recognized by previous authors, pointing to dextral activity of the GKDFS up to the end of the Miocene, when the fault zone flipped to left-lateral strike-slip motions.

Considering the continuity of the exposed portion of the AFS and its dimensions and related structures, we propose that this fault may directly represent one of the main branches of the dextral GKDFS, which was active before the Pliocene time interval. The GKDFS represents a well-defined example of the large dextral shear zone bordering the northern boundary of the CEIM during most of the Cenozoic connecting the central part of the fault, the Doruneh segment, with its westernmost termination in the Ashin area.

Integrating our structural data with previous structural analyses on the GKDFS, available paleomagnetic data and the updated information on the displaced fragments of the Paleotethyan and Neotethyan ophiolites, we observe a good coincidence between block rotations and displacements of the Paleotethys and Neotethys units, following a simple geometrical model. According to this model, we restore these units to their previous positions, in response to the CCW rotations occurred along vertical axes (Mattei et al., 2015). The larger displacements shown by the Paleotethys units may be explaine d by the larger rotations occurring since the Triassic, with respect to the smaller displacements suffered by the Upper Cretaceous Neotethyan ophiolites.

Several uncertainties on large block rotations and displacement of crustal blocks remain to be better investigated, especially with concern to the evolution of the poorly known regions of the Sistan and Makran orogens and to their role in the deformation of Central Iran.

Finally, we consider that at least part of the observed block rotations in Central Iran may be directly related to a large-scale phenomenon of escape tectonics related to the westward extrusion of the Cimmerian blocks of Afghanistan and Central Iran to the south of the pre-Pliocene dextral GKDFS – Herat Fault Zone, resulting from the indentation of India into Eurasia.

Acknowledgments

We are deeply indebted with the Geological Survey of Iran of Teheran, for providing invaluable help during fieldwork in Arusan. We are also grateful with the owner of the Potash Mine house, who kindly hosted us during several weeks of work in the area.

The present project has been funded by the DARIUS PROGRAMME: “The Late Paleozoic to Eo-Cimmerian Orogenic Complexes of Central Iran: a Still Unsolved Enigma” and by the PRIN20102011 Italian MIUR project: “Birth and death of oceanic basins: geodynamic processes from rifting to continental collision in Mediterranean and Circum-Mediterranean orogens”. It was carried out in the frame of a Memorandum of Understanding between the Geological Survey of Iran and the

Department of Earth and Environmental Sciences of the Milano-Bicocca University.

We are in debt to Marcel Sosson and an anonymous reviewer that helped us to improve a first version of the paper. We also wish to thanks Laurent Jolivet for editorial handling and useful comments.

Original data used for geological-structural interpretation and paleostress reconstruction are available in the Mendeley Data free -access repository (doi: 10.17632/n7x9bpc292.1). Data include a geological map with the localization of all the measurement sites, a .kml file of measurement sites, a georeferenced false color composite image of the study area elaborated from satellite ASTER images, a portfolio of fault planes with kinematic indicators as observed in outcrops, fault slip data used for paleostress calculations.

References

Alavi, M. (1991). Sedimentary and structural characteristics of the Paleo-Tethys remnants in northeastern Iran. *Geological Society of America Bulletin*, *103(8)*, 983-992.

Alavi, M., Vaziri, H., Seyed Enami, K., & Lasemi, Y. (1997). The Triassic and associated rocks of the Nakhlak and Aghdarband areas in central and northeastern Iran as remnants of the southern Turanian active continental margin. *Geological Society of America Bulletin, 109*, 1563-1575.

Allen, M. B., Ghassemi, M. R., Shahrabi, M., & Qorashi, M. (2003). Accommodation of late Cenozoic oblique shortening in the Alborz range, northern Iran. *Journal of Structural Geology*, *25*(5), 659-672.

Angelier, J. (1984). Tectonic analysis of fault slip data sets. *Journal of Geophysical Research, 89*, 5835-5848.

Angelier, J. (1990). Inversion of field data in fault tectonics to obtainthe regional stress-III. A new rapid direct inversion method byanalytical means. *Geophysical Journal International, 103*, 363-376.

Angelier, J. (2002). Inversion of earthquake focal mechanisms to obtain the seismotectonic stress IV—a new method free of choice among nodal planes. *Geophysical Journal International*, *150*(3), 588-609.

Bagheri, S. & Gol, S. D. (2021). The eastern Iranian Orocline. *Earth Science Reviews, 250*, doi.org/10.1016/j.earscirev.2020.103322.

Bagheri, S., & Stampfli, G. M. (2008). The Anarak, Jandaq and Posht-e-Badam metamorphic complexes in central Iran: New geological data, relationships and tectonic implications. *Tectonophysics, 451*, 123-155.

Bagheri, S., Madhanifard, R., & Zahabi, F. (2017). Kinematics of the Great Kavir fault inferred from a structural analysis of the Pees Kuh Complex, Jandaq area, central Iran. *Tectonic Evolution, Collision, and Seismicity of Southwest Asia: In Honor of Manuel Berberian's Forty-Five Years of*

Research Contributions, *525*, 213-227.

Balini, M., Nicora, A., Berra F., Garzanti, F., Levera, M., Mattei M., et al. (2009). The Triassic stratigraphic succession of Nakhlak (central Iran), a record from an active margin. In: M.F. Brunet, M. Wilmsen, & J.W. Granath (Eds.), *South Caspian to Central Iran Basins* (Vol. 312, pp. 287-321). Geological Society of London Special Publications.

Balini, M., Nicora, A., Zanchetta, S., Zanchi, A., Marchesi, R., Vuolo, I., et al. (2019). Olenekian to Early Ladinian stratigraphy of the western part of the Aghdarband window (Kopeh-dag, NE Iran). *Rivista Italiana di Paleontologia e Stratigrafia*, *125(1),* 283-315.

Barrier, E., & Vrielynck, B. (2008). Palaeotectonic Maps of the Middle East, Atlas of 14Maps. CGMW/CCGM, Paris, France.

Berra, F., Zanchi, A., Angiolini, L., Vachard, D., Vezzoli, G., Zanchetta, S., et al. (2017). The upper Palaeozoic Godar-e-Siah Complex of Jandaq: evidence and significance of a North Palaeotethyan succession in Central Iran. *Journal of Asian Earth Sciences*, *138*, 272-290.

Bonnet, G., Agard, P., Angiboust, S., Monié, P., Jentzer, M., Omrani, J., et al. (2018). Tectonic slicing and mixing processes along ther subduction interface: The Sistan example (Eastern Iran). *Lithos*, *310311*, 269-287.

Bröcker, M., Rad, G. F., Burgess, R., Theunissen, S., Paderin, I., Rodionov, N., & Salimi, Z. (2013). New age constraints for the geodynamic evolution of the Sistan Suture Zone, eastern Iran. *Lithos*, *170*, 17-34.

Carey, E., & Brunier, B. (1974). Numerical-analysis of an elementary mechanical model applied to study of a population of faults. *Comptes Rendus Hebdomadaires des Seances de l'Academie des Sciences Serie D*, *279*(11), 891-894.

Davoudzadeh, M., & Schmidt, K. (1981). Contribution to the paleogeography and stratigraphy of the Upper Triassic to Middle Jurassic of Iran. *Neues Jahrbuch für Geologie und Paläontologie. Abhandlungen*, *162*(2), 137-163.

Davoudzadeh, M., & Weber -Diefenbach, K. (1997). Paleogeography, stratigraphy, and tectonics of the tertiary of Iran. *Neues Jahrbuch für Geologie und Paläontologie-Abhandlungen*, 33-67.

Delvaux, D., & Sperner, B. (2003). Stress tensor inversion from fault kinematic indicators and focal mechanism data: the TENSOR program. In: D. Nieuwland (Eds.), *New Insights into Structural Interpretation and Modelling* (Vol. 212, pp. 75-100). Geological Society, London, Special Publications.

Díaz-Azpiroz, M., Barcos, L., Balanyá, J. C., Fernández, C., Expósito, I., & Czeck, D. M. (2014). Applying a general triclinic transpression model to highly partitioned brittle-ductile shear zones: A

case study from the Torcal de Antequera massif, external Betics, southern Spain. *Journal of Structural Geology*, *68*, 316-336.

Dolati, A., & Burg, J.P. (2013). Preliminary fault analysis and paleostress evolution in the Makran Fold-and-Thrust Belt in Iran. In: K. Al Hosani et al. (Eds.), *Lithosphere Dynamics and Sedimentary Basins: The Arabian Plate and Analogues*, Frontiers in Earth Sciences.

Farbod, Y., Bellier, O., Shabanian, E., & Abbassi, M. R. (2011). Geomorphic and structural variations along the Doruneh Fault System (central Iran). *Tectonics*, *30*(6), TC6014, doi:10.1029/2011TC002889.

Farbod, Y., Shabanian, E., Bellier, O., Abbassi, M. R., Braucher, R., Benedetti, L., et al. (2016). Spatial variations in late Quaternary slip rates along the Doruneh Fault System (Central Iran). *Tectonics*, *35*(2), 386-406.

Fossen, H., & Cavalcante, G. C. G. (2017) Shear zones—a review. *Earth Science Reviews, 171*, 434-455.

Fossen, H., & Tikoff, B. (1993). The deformation matrix for simultaneous pure shear, simple shear, and volume change, and its application to transpression/transtension tectonics. *Journal of Structural Geology, 15*, 413-422.

Fossen, H., & Tikoff, B. (1998). Extended models of transpression and transtension, and application to tectonic settings. In: R.E. Holdsworth, R.A. Strachan, & J.F. Dewey (Eds.), *Continental Transpressional and Transtensional Tectonics* (Vol. 135, pp. 15-33). Geological Society, London, Special Publications.

Fossen, H., Tikoff, B., & Teyssier, C. (1994). Strain modelling of transpressional and transtensional deformation. *Norsk Geologisk Tidsskrift, 74*, 134-145.

Freund, R. (1970). Rotation of strike slip faults in Sistan, southeast Iran. *The Journal of Geology*, *78*(2), 188-200.

Guest, B., Axen, G. J., Lam, P. S., & Hassanzadeh, J. (2006). Late Cenozoic shortening in the west central Alborz Mountains, northern Iran, by combined conjugate strike-slip and thin-skinned deformation. *Geosphere*, *2*(1), 35-52.

Hassanzadeh, J., & Wernicke, B. P. (2016). The Neotethyan Sanandaj‐Sirjan zone of Iran as an archetype for passive margin‐arc transitions. *Tectonics*, *35*(3), 586-621.

Javadi, H. R., Esterabi Ashtiani, M., Guest, B., Yassaghi, A., Ghassemi, M. R., Shahpasandzadeh, M., & Naeimi, A. (2015). Tectonic reversal of the western Doruneh Fault System: Implications for Central Asian tectonics. *Tectonics, 34*, 2034-2051.

Javadi, H. R., Ghassemi, M. R., Shahpasandzadeh, M., Guest, B., Ashtiani, M. E., Yassaghi, A., & Kouhpeyma M. (2013). History of faulting on the Doruneh Fault System: implications for the kinematic changes of the Central Iranian Microplate. *Geological Magazine, 150*, 651-672.

Jentzer, M., Fournier, M., Agard, P., Omrani, J., Khatib, M. M., & Whitechurch, H. (2017). Neogene to Present paleostress field in Eastern Iran (Sistan belt) and implications for regional geodynamics. *Tectonics*, *36*(2), 321-339.

Jentzer, M., Whitechurch, H., Agard, P., Ulrich, M., Caron, B., Zarrinkoub, M. H., Kohansal, R., Miguet, L., Omrani, J., & Fournier, M. (2020). Late Cretaceous calc-alkaline and adakitic magmatism in the Sistan suture zone (Eastern Iran): Implications for subduction polarity and regional tectonics. *Journal of Asian Earth Sciences*, *204*, 104588.

Kargaranbafghi, F., Neubauer, F., & Genser, J. (2011). Cenozoic kinematic evolution of southwestern Iran: Strain partitioning and accommodation of Arabia–Eurasia convergence. *Tectonophysics*, *502(1-2)*, 221-243.

Kargaranbafghi, F., Neubauer, F., Genser, J., Faghih, A., & Kusky, T. (2012). Mesozoic to Eocene ductile deformation of western Central Iran: From Cimmerian collisional orogeny to Eocene exhumation. *Tectonophysics*, *564*, 83-100.

Karimpour, M. H., Farmer, G. L., & Stern, C. R. (2010). Geochronology, radiogenic isotope geochemistry, and petrogenesis of Sangbast Paleo-Tethys monzogranite, Mashhad, Iran. *Iranian Journal of Crystallography and Mineralogy*, *17(4)*, 703-715.

Kent, D. V., & Muttoni, G. (2020). Pangea B and the Late Paleozoic Ice Age. *Palaeogeography, Palaeoclimatology, Palaeoecology*, 109753, https://doi.org/10.1016/j.palaeo.2020.109753.

Mattei, M., Cifelli, F., Alimohammadian, H., Rashid, H., Winkler, A., & Sagnotti, L. (2017). Oroclinal bending in the Alborz Mountains (Northern Iran): New constraints on the age of South Caspian subduction and extrusion tectonics. *Gondwana Research*, *42*, 13-28.

Mattei, M., Cifelli, F., Muttoni, G., & Rashid, H. (2020). The role of active strike-slip faults and opposite vertical axis rotations in accommodating Eurasia-Arabia shortening in Central Iran**.** Tectonophysics, 774, 228243, 10.1016/j.tecto.2019.228243.

Mattei, M., Cifelli, F., Muttoni, G., & Rashid, H. (2015). Post-Cimmerian (Jurassic-Cenozoic) paleogeography and vertical axis tectonic rotations of Central Iran and the Alborz Mountains. *Journal of Asian Earth Sciences, 102*, 92-101.

Mattei, M., Cifelli, F., Muttoni, G., Zanchi, A., Berra, F., Mossavvari, F., & Eshraghi, S. A. (2012). Neogene block-rotation in Central Iran: evidence from paleomagnetic data. *Geological Society of America Bulletin, 124,* 943-956.

Mattei, M., Visconti, A. L., Cifelli, F., Nozaem, R., Winkler, A., & Sagnotti, L. (2019). Clockwise paleomagnetic rotations in northeastern Iran: Major implications on recent geodynamic evolution of outer sectors of the Arabia-Eurasia collision zone. *Gondwana Research*, *71*, 194-209.

Means, W. D., Hobbs, B. E., Lister, B. E., & Williams, P. F. (1980). Vorticity and non-coaxiality in progressive deformations. *Journal of Structural Geology, 2*, 371-378.

Mirnejad, H., Lalonde, A. E., Obeid, M., & Hassanzadeh, J. (2013). Geochemistry and petrogenesis of Mashhad granitoids: An insight into the geodynamic history of the Paleo-Tethys in northeast of Iran. *Lithos*, *170*, 105-116.

Moghadam, H. S., Khademi, M., Hu, Z., Stern, R. J., Santos, J. F., & Wu, Y. (2015). Cadomian (Ediacaran–Cambrian) arc magmatism in the ChahJam–Biarjmand metamorphic complex (Iran):

Magmatism along the northern active margin of Gondwana. *Gondwana Research*, *27(1)*, 439-452.

Molnar, P., & Tapponnier, P. (1975). Cenozoic tectonics of Asia: effects of a continental collision. *Science*, *189*(4201), 419-426.

Morin, J., Jolivet, M., Robin, C., Heilbronn, G., Barrier, L., Bourquin, S., & Jia, Y. (2018). Jurassic paleogeography of the Tian Shan: An evolution driven by far-field tectonics and climate. *EarthScience Reviews, 187*, 286-313.

Mount, V. S. & Suppe, J. (1987). State of stress near the San Andreas fault: Implications for wrench tectonics. *Geology*, *15(12)*, 1143-1146.

Muttoni, M., Mattei, M., Balini, M., Zanchi, A., Gaetani, M., & Berra, F. (2009). The drift history of Iran from the Ordovician to the Triassic. In: M.F. Brunet, M. Wilmsen, & J.W. Granath (Eds.), *South Caspian to Central Iran Basins* (Vol. 312, pp. 7-29). Geological Society of London Special Publications.

Navabpour, P., Angelier, J., & Barrier, E. (2007). Cenozoic post-collisional brittle tectonic history and stress reorientation in the High Zagros Belt (Iran, Fars Province). *Tectonophysics*, *432*(1-4), 101131.

Nozaem, R., Mohajjel, M., Rossetti, F., Della Seta, M., Vignaroli, G., Yassaghi, A., Salvini, F., and Eliassi, M., 2013, Post-Neogene right-lateral strike-slip tectonics at the north-western edge of the Lut block (Kuh-eSarhangi fault), central Iran. *Tectonophysics*, *589*, 220–233.

Omrani, H., Moazzen, M., Oberhänsli, R., Altenberger, U., & Lange, M. (2013). The Sabzevar blueschists of the North-Central Iranian micro-continent as remnants of the Neotethys-related oceanic crust subduction. *International Journal of Earth Sciences, 102*(5), 1491-1512.

Onderdonk, N. W. (2005). Structures that accommodated differential vertical axis rotation of the western Transverse Ranges, California. *Tectonics*, *24(4)*, TC4018.

J.‐P., & Barquins, M. (1988). Can natural faults propagate under Mode II conditions?, *Tectonics*, *7(6),* 1243-1256, doi:10.1029/TC007i006p01243

Pirnia, T., Saccani, E., Torabi, G., Chiari, M., Goričan, Š., & Barbero, E. (2020). Cretaceous tectonic evolution of the Neo-Tethys in Central Iran: Evidence from petrology and age of the Nain-Ashin ophiolitic basalts. *Geoscience Frontiers*, *11*(1), 57-81.

Ramezani, J., & Tucker, R. D. (2003). The Saghand region, central Iran: U-Pb geochronology, petrogenesis and implications for Gondwana tectonics. *American Journal of Science*, *303*(7), 622665.

Romanko, E., 1969). Mesr 6957 and Arusan 7059 sheets of the Geological Map of Iran at 1: 100,000

Ron, H., Freund, R., Garfunkel, Z., & Nur, A. (1984). Block rotation by strike‐slip faulting: Structural and paleomagnetic evidence. *Journal of Geophysical Research: Solid Earth*, *89*(B7), 6256-

Rossetti, F., Nozaem, R., Lucci, F., Vignaroli, G., Gerdes, A., Nasrabadi, M., & Theye, T. (2015). Tectonic setting and geochronology of the Cadomian (Ediacaran-Cambrian) magmatism in central Iran, Kuh-e-Sarhangi region (NW Lut Block). *Journal of Asian Earth Sciences*, *102*, 24-44. Ruttner, A. W. (1993). Southern borderland of Triassic Laurasia in north-east Iran. *Geologische Rundschau*, *82(1)*, 110-120.

Ruttner, A. W., Brandner, R., & Kirchner, E. (1991). Geology of the Aghdarband area (kopet Dagh, NE-Iran). *Abhandlungen der Geologischen Bundesanstalt*, *38*, 7-79.

Shabanian, E., Bellier, O., Siame, L., Arnaud, N., Abbassi, M. R., & Cochemé, J.‐J. (2009). New tectonic configuration in NE Iran: active strike‐slip faulting between the Kopeh Dagh and Binalud mountains. *Tectonics*, *28*(5), TC5002, doi: 10.1029/2008TC002444.

Sharkovski, M., Susov, M., & Krivyakin, B. (1984). Geology of the Anarak area (central Iran). Explanatory text of the Anarak quadrangle map 1:250.000. Geological Survey of Iran, V/O "Technoexport" USSR Ministry of Geology, Reports, TE/No. 19, 143 pp. Moscow.

Sheikholeslami, M. R., & Kouhpeyma, M. (2012). Structural analysis and tectonic evolution of the eastern Binalud Mountains, NE Iran. *Journal of Geodynamics*, *61*, 23-46.

Sheikholeslami, M. R., Oberhänsli, R., & Ghassemi, M. R. (2019). Transpression tectonics in the eastern Binalud Mountains, northeast Iran; Insight from finite strain analysis, vorticity and $^{40}Ar/^{39}Ar$ dating. *Journal of Asian Earth Sciences*, *179*, 219-237.

Shirdashtzadeh, N., Torabi, G., & Schaefer, B. (2018). A magmatic record of Neoproterozoic to Paleozoic convergence between Gondwana and Laurasia in the northwest margin of the Central-East Iranian Microcontinent. *Journal of Asian Earth Sciences*, *166*, 35-47.

Soffel, H. C., Schmidt, S., Davoudzadeh, M., & Rolf, C. (1996). New palaeomagnetic data from Central Iran and a Triassic palaeoreconstruction. *Geologische Rundschau*, *85*(2), 293-302.

Sonder, L. J., Jones, C. H., Salyards, S. L., & Murphy, K. M. (1994). Vertical axis rotations in the Las Vegas Valley Shear Zone, southern Nevada: Paleomagnetic constraints on kinematics and dynamics of block rotations. *Tectonics*, *13(4)*, 769-788.

Stöcklin, J. (1974). Possible ancient continental margins in Iran. In The geology of continental margins (pp. 873-887). Springer, Berlin, Heidelberg.

Storetvedt, K. M. (1974). A possible large-scale sinistral displacement along the Great Glen Fault in Scotland. *Geological Magazine*, *111(1)*, 23-30.

Storetvedt, K. M. (1987). Major late Caledonian and Hercynian shear movements on the Great Glen Fault. *Tectonophysics*, *143(4)*, 253-267.

Storti, F., Holdsworth, R. E., & Salvini, F. (2003). Intraplate strike-slip deformation belts. *Geological Society, London, Special Publications*, *210*(1), 1-14.

Tadayon, M., Rossetti, F., Zattin, M., Calzolari, G., Nozaem, R., Salvini, F., et al. (2019). The long‐term evolution of the Doruneh Fault region (Central Iran): A key to understanding the spatio‐temporal tectonic evolution in the hinterland of the Zagros convergence zone. *Geological Journal*, *54(3),* 1454-1479.

Tadayon, M., Rossetti, F., Zattin, M., Nozaem, R., Calzolari, G., Madanipour, S., & Salvini, F. (2017). The post‐eocene evolution of the Doruneh Fault region (central Iran): The intraplate response to the Reorganization of the Arabia‐Eurasia collision zone. *Tectonics*, *36(12),* 3038-3064.

Tapponnier, P., Lacassin, R., Leloup, P. H., Schärer, U., Dalai, Z., Haiwei, W., Xiaohan, L., Shaocheng, J., Lianshang, Z., & Jiayou, Z. (1990). The Ailao Shan/Red River metamorphic belt: tertiary left-lateral shear between Indochina and South China. *Nature*, *343*(6257), 431-437. Torabi, G. (2009). Chromitite potential in mantle peridotites of the Jandaq ophiolite (central Iran). *Comptes Rendus Geoscience*, *341*(12), 982-992.

Torabi, G. (2012). Late Permian post‐ophiolitic trondhjemites from Central Iran: a mark of subduction role in growth of Paleozoic continental crust. *Island Arc*, *21*(3), 215-229.

Truesdell, C. (1953). Two measures of vorticity. *Journal of Rational Mechanics and Analysis, 2*, 173-217.

Walker, R., & Jackson, J. (2004). Active tectonics and late Cenozoic strain distribution in central and eastern Iran. *Tectonics*, *23(5)*, TC5010.

Weijermars, R. (1991). The role of stress in ductile deformation. *Journal of Structural Geology, 13*, 1061-1078.

Wilmsen, M., Berensmeier, M., Fürsich, F. T., Majidifard, M. R., & Schlagintweit, F. (2018). A Late Cretaceous epeiric carbonate platform: the Haftoman Formation of central Iran. *Facies*, *64(2)*, 1-24.

Wilmsen, M., Berensmeier, M., Fürsich, F. T., Schlagintweit, F., Hairapetian, V., Pashazadeh, B., & Majidifard, M. R. (2020). Mid-Cretaceous biostratigraphy (ammonites, inoceramid bivalves and foraminifers) at the eastern margin of the Anarak Metamorphic Complex (Central Iran). *Cretaceous Research*, *110*, 104411.

Wilmsen, M., Fürsich, F. T., & Majidifard, M. R. (2015). An overview of the Cretaceous stratigraphy and facies development of the Yazd Block, western Central Iran. *Journal of Asian Earth Sciences*, *102*, 73-91.

Zanchetta, S., Berra, F., Zanchi, A., Bergomi, M., Caridroit, M., Nicora, M., & Heidarzadeh, G. (2013). The record of the Late Palaeozoic active margin of the Palaeotethys in NE Iran: Constraints on the Cimmerian orogeny. *Gondwana Research, 24*, 1237-1266.

Zanchetta, S., Malaspina, N., Zanchi, A., Benciolini, L., Martin, S., Javadi, H. R, & Kouhpeyma, M. (2018). Contrasting subduction–exhumation paths in the blueschists of the Anarak Metamorphic Complex (Central Iran). *Geological Magazine, 155(2)*, 316-334. doi:10.1017/S0016756817000218

Zanchetta, S., Zanchi, A., Montemagni C., Berra, F. &, Mattei, M. (2021), Cenozoic dextral shearing along the Arusan sector of the Great Kavir – Doruneh Fault System (Central Iran). Mendeley Data, V1, doi: 10.17632/n7x9bpc292.1.

Zanchi, A., Berra, F., Mattei, M., Ghassemi, M. R., & Sabouri, J. (2006). Inversion tectonics in central Alborz, Iran. *Journal of Structural Geology*, *28*(11), 2023-2037.

Zanchi, A., Malaspina, N., Zanchetta, S., Berra, F., Benciolini, L., Bergomi, M., et al. (2015). The Cimmerian accretionary wedge of Anarak, Central Iran. *Journal of Asian Earth Sciences, 102*, 45-72.

Zanchi, A., Zanchetta, S., Balini, M., & Ghassemi, M. R. (2016). Oblique convergence during the Cimmerian collision: Evidence from the Triassic Aghdarband Basin, NE Iran. *Gondwana Research, 38*, 149-170

Zanchi, A., Zanchetta, S., Berra, F., Mattei, M., Garzanti, E., Molyneux, S., et al. (2009a). The EoCimmerian (Late? Triassic) orogeny in north Iran. In: M.F. Brunet, M. Wilmsen, & J.W. Granath (Eds.), *South Caspian to Central Iran Basins* (Vol. 312, pp. 31-55). Geological Society of London Special Publications.

Zanchi, A., Zanchetta, S., Garzanti, E., Balini, M., Berra, F., Mattei, M., & Muttoni, G. (2009b). The Cimmerian evolution of the Nakhlak-Anarak area, central Iran, and its bearing for the reconstruction of the history of the Eurasian margin. In: M.F. Brunet, M. Wilmsen, & J.W. Granath (Eds.), *South*

Caspian to Central Iran Basins (Vol. 312, pp. 261-286). Geological Society of London Special Publications.

Zarrinkoub, M. H., Pang, K. N., Chung, S. L., Khatib, M. M., Mohammadi, S. S., Chiu, H. Y., & Lee, H. Y. (2012). Zircon U–Pb age and geochemical constraints on the origin of the Birjand ophiolite, Sistan suture zone, eastern Iran. *Lithos*, *154*, 392-405.

Zoback, M. L. (1992). First- and second-order patterns of stress in the lithosphere: The World Stress Map Project. *Journal of Geophysical Research: Solid Earth, 97(B8), 11703-11728.*

Figure captions

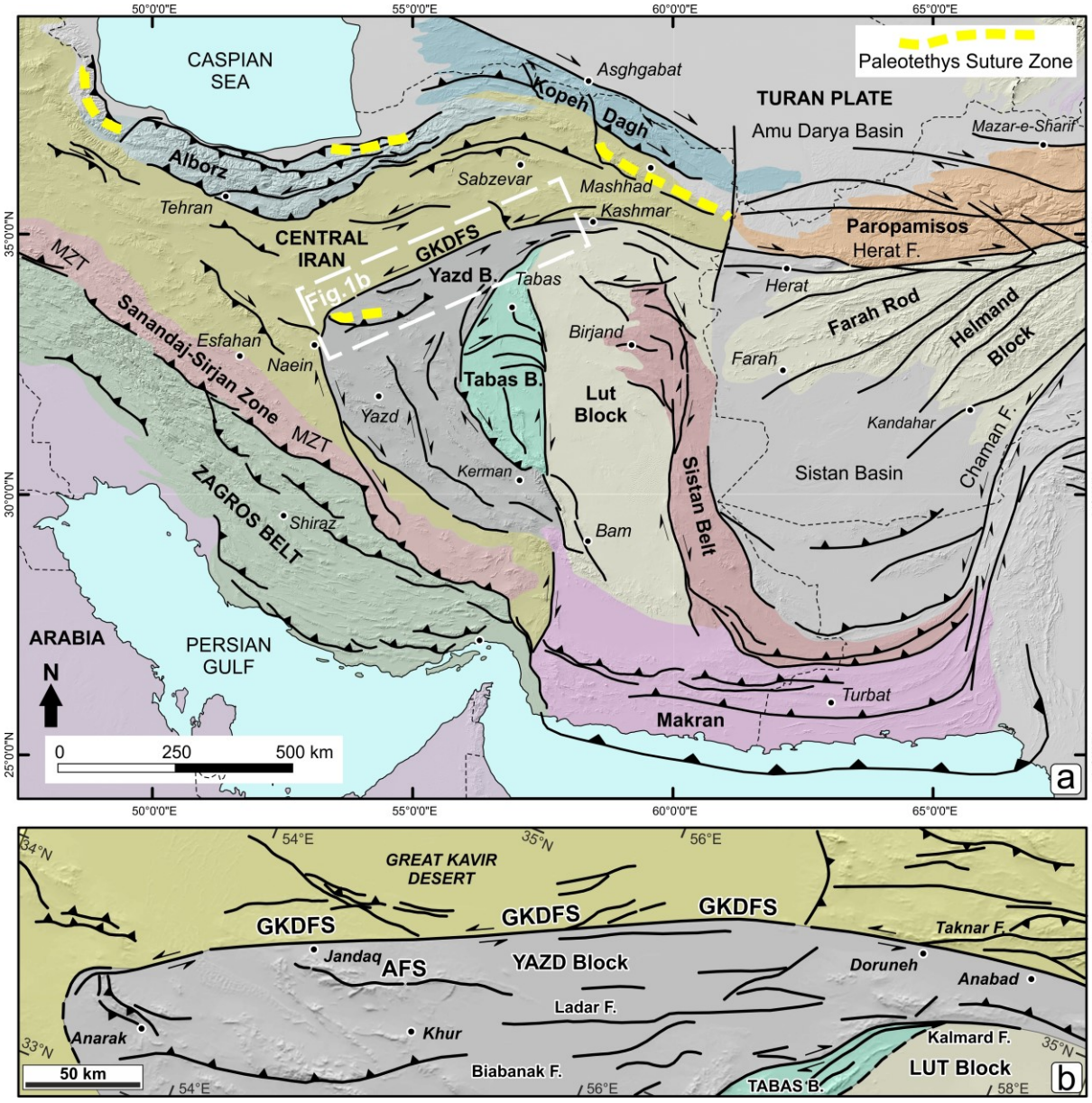

Figure 1. (a) General of map Iran and surrounding areas extending to Afghanistan with the main fault zones. (b) Simplified structural map of the Great Kavir Doruneh Fault System (GKDFS), location in Figure 1a; modified from Javadi et al. (2013). AFS: Arusan Fault System.

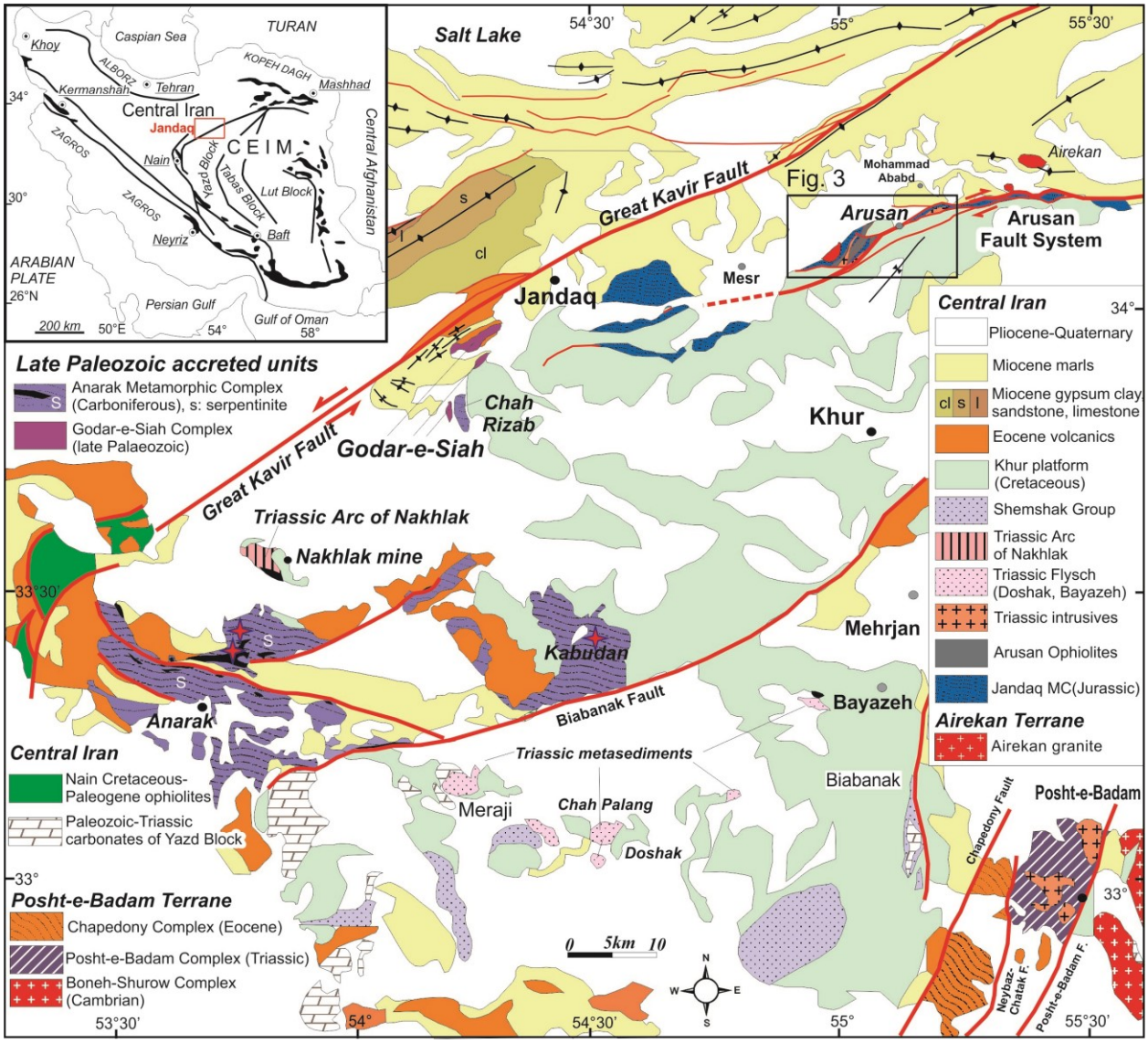

Figure 2. Simplified structural map of the NW corner of Central Iran, with location of Figure 3; modified from Bagheri & Stampfli (2008) and from Berra et al. (2017), according to our original information. CEIM: Central Eastern Iran Microplate.

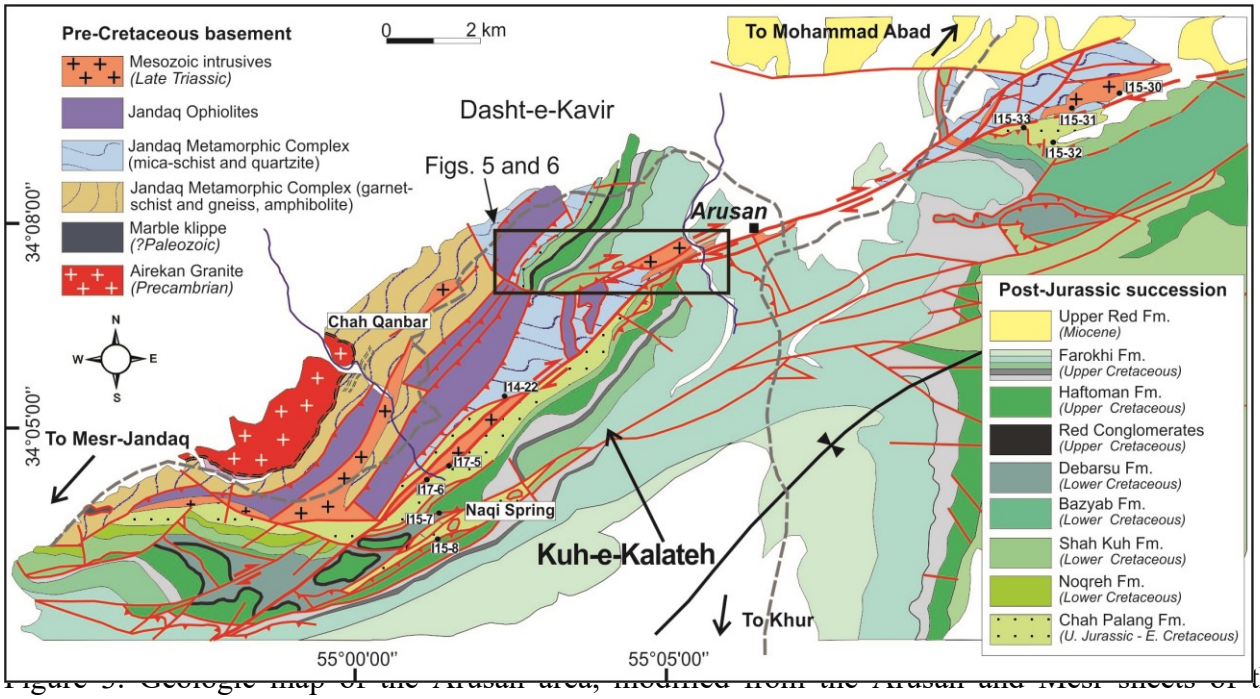

Figure 3. Geologic map of the Arusan area, modified from the Arusan and Mesr sheets of the Geological map of Iran (1:100,000; Romanko et al., 1969) according to our field survey. The location of some structural sites not present in the following maps are reported. The square shows the position of Figures 5 and 6.

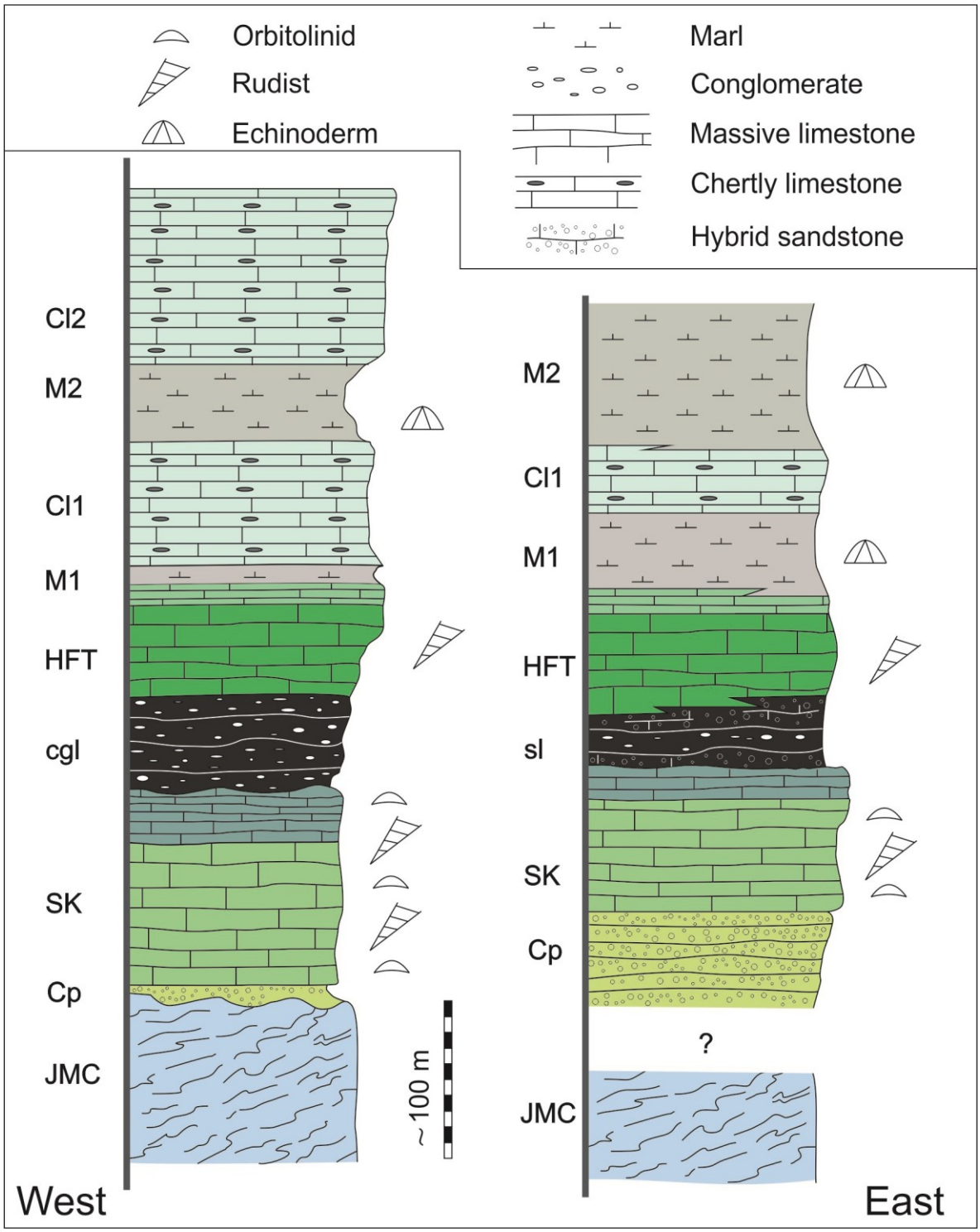

Figure 4. Synthetic stratigraphic logs of the Arusan area. Bas: Arusan Metamorphic Complex; Cp: Chah Palang Formation; SK: Shah Kuh Formation; cgl: red conglomerate; sl: hybrid limestone with sandstone andmicroconglomerates; HFT: Haftoman Formation; Farokhi Formation including M1: lower marls; CL1: lower cherty limestone; M2: upper marls; CL2: upper cherty limestone.

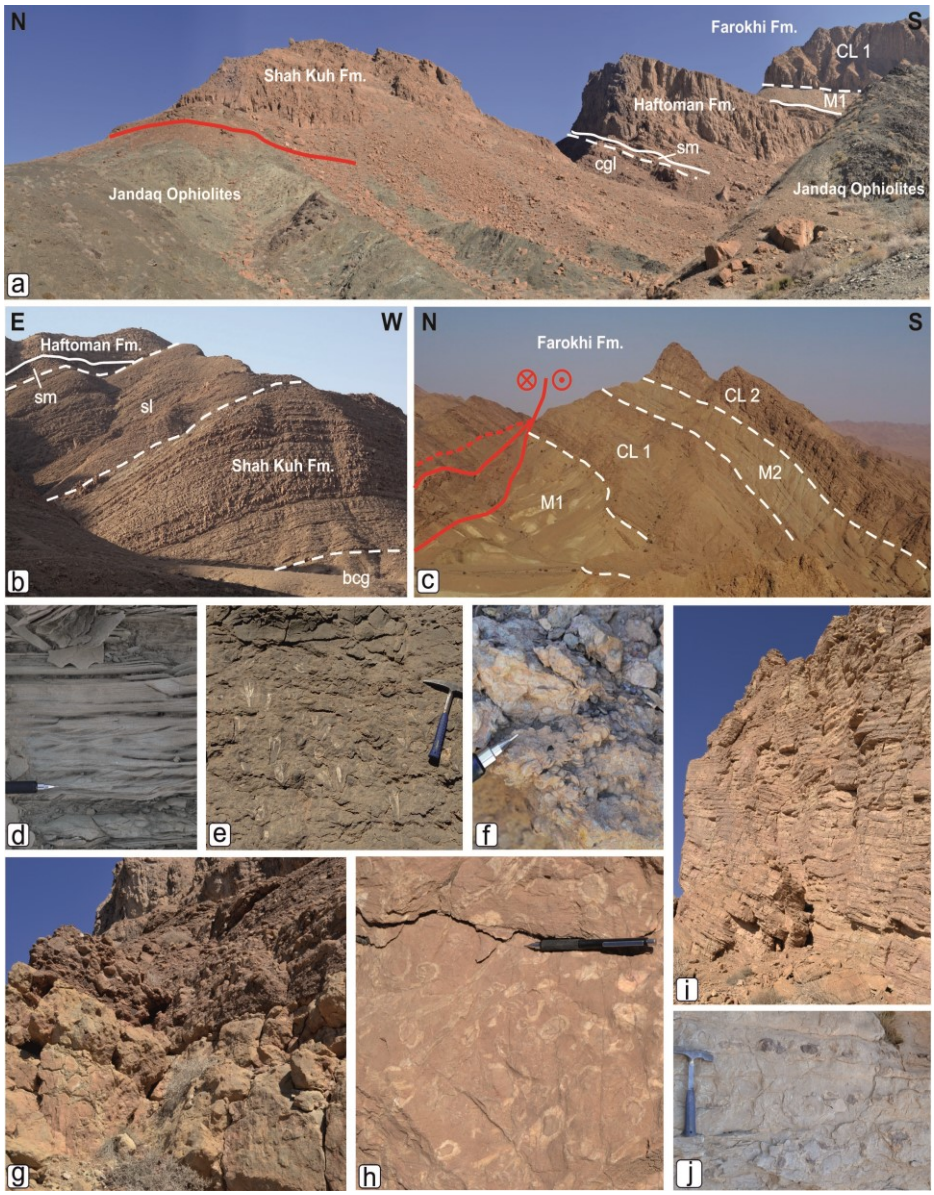

Figure 5. The Cretaceous succession exposed north of Kuhr close to Arusan. (a) View of the Cretaceous succession non-conformably covering the metamorphic basement close to cross section E-E' (Figure 7): a thick conglomerate unit (referred to as Haftoman Fm. by Wilmsen et al. 2015) is present between the Shah Kuh Formation and the limestone of the Haftoman Formation. (b) View of the succession on the northwestern side of the study area, where the conglomeratic unit (Figure 5a) is not present. (c) The Farokhi Formation, south of a major branch of the AFS close to the Naqi Spring (Figure 3); note the alternation of marly and calcareous units. (d) Current ripples in quartz-rich sandstone of the Chah Palang Formation. (e): rudists in life position in the Shah Kuh Formation. (f) Bioclastic silty rudstone with Orbitolinid macroforaminifera in the upper part of the Shah Kuh Formation. (g) Erosional surface between the massive limestone of the Shah Kuh Formation and the overlying, poorly selected conglomerates with carbonate clasts. (h) Typical aspect of the rudist limestone of the Haftoman Formation. (i) Bedded fine-grained packstone with chert of the lower cherty limestone marking the drowning recorded by the Haftoman Formation. (j) Close-up view of chert nodules in fine-grained pelagic mudstone/wakestone of the upper cherty limestone.
bcg: conglomerate at the base of the Shah Kuh Formation; sl: silty limestone, sm: silty marl (at the base of the Haftoman Fm.); cgl: red conglomerate (Haftoman Fm. sensu Wilmsen et al., 2015); Farokhi Formation including M1: lower marls; CL1: lower cherty limestone; M2: upper marls; CL2: upper cherty limestone.

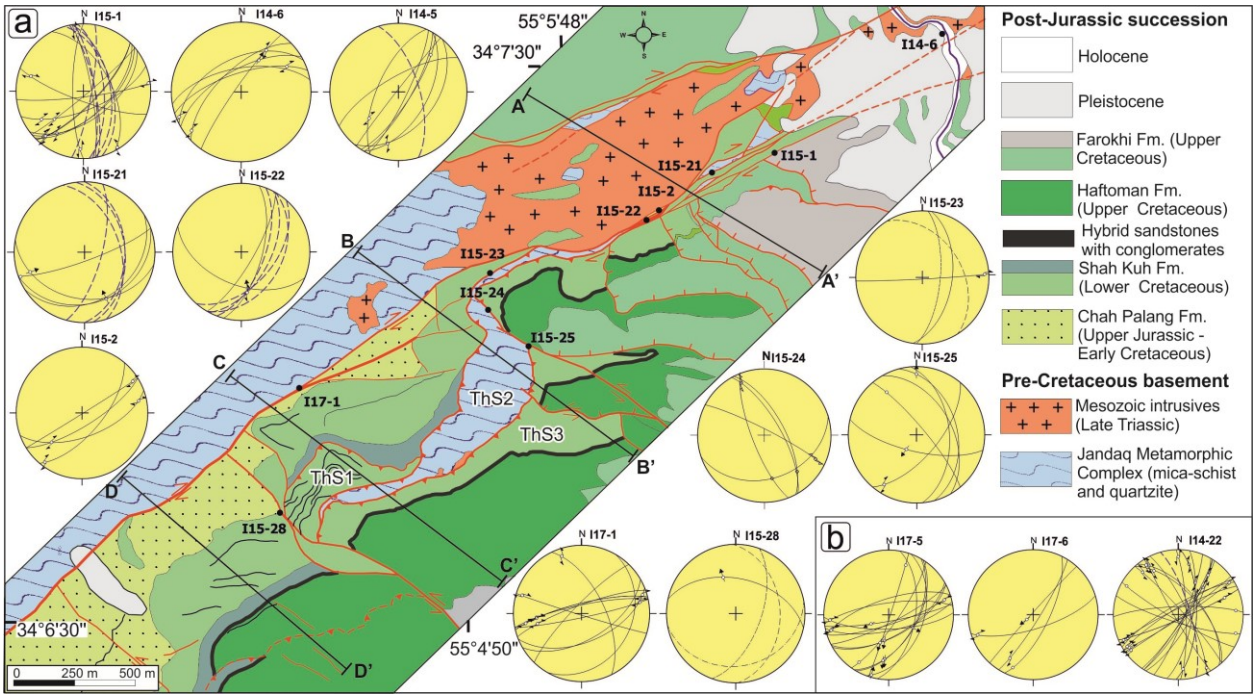

Figure 6. (a) Geological map of the eastern branch of the Arusan Fault; the map is based on our original structural and stratigraphic analyses. We also used ASTER satellite imagery (see additional materials) and it was drown in Google Map. Location of the structural observations and the traces of cross sections are reported. Stereographic projections are Schmidt, lower hemisphere; faults are shown as cyclographic projections with striations and sense of motion when available; blue and black dashed lines are respectively cleavage and bedding. (b) Three plots showing data located out of the map to the south showing faults measured along the Eastern Arusan Fault; location in Figure 12. ThS: Thrust Sheet.

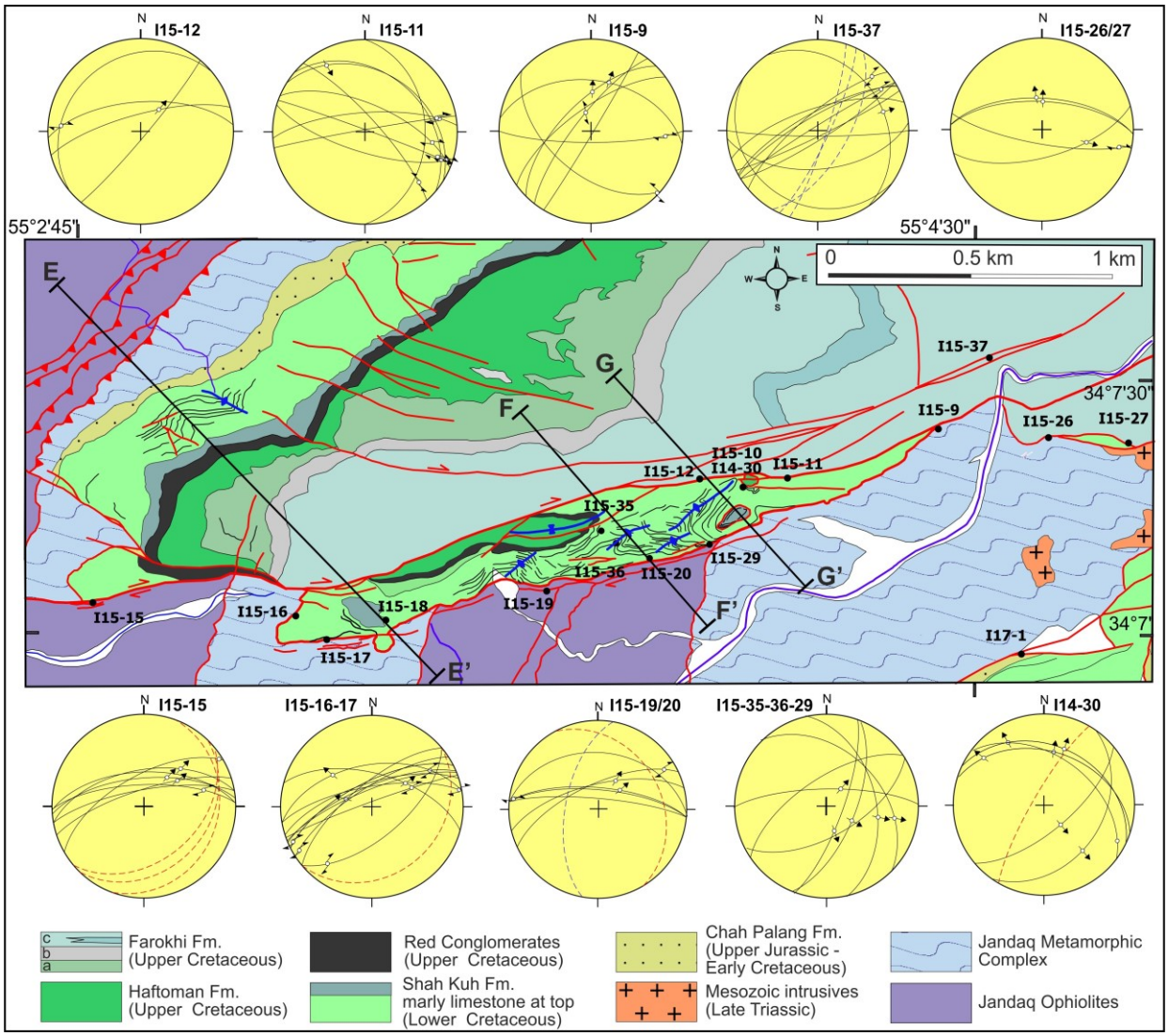

Figure 7. Geological map of the western branch of the Arusan Fault. Symbols as in Figure 6.

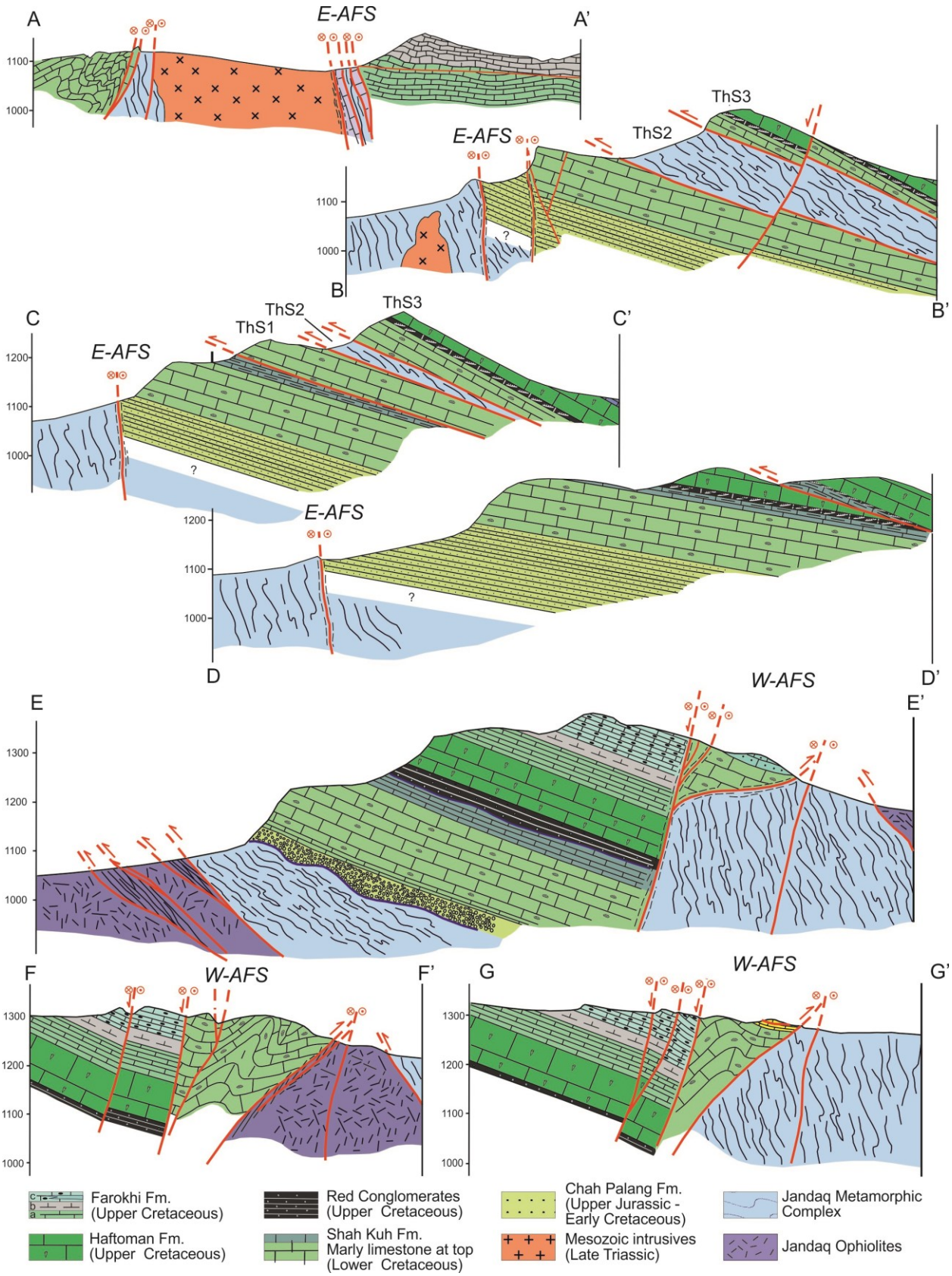

Figure 8. Serial geological sections across the two branches of the Arusan Fault System. Traces of sections A to D are reported in Figure 5; traces of sections E to G are shown in Figure 7. E-AFS: Eastern Arusan Fault System; W-AFS: Western Arusan Fault System; ThS: Thrust Sheet.

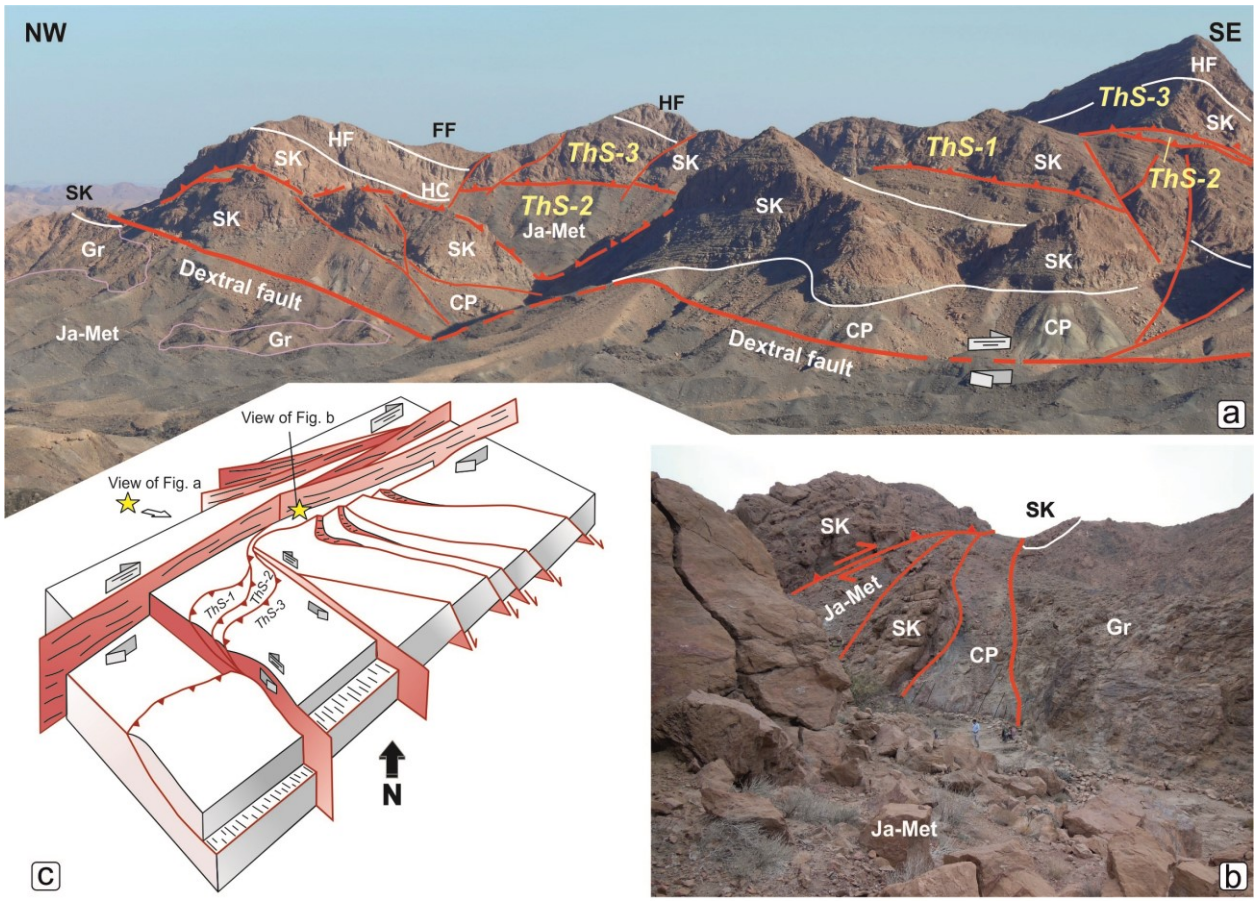

Figure 9. (a) Panoramic view from SSW to NNE of the eastern branch of the AFS, showing field relationships among thrust and strike-slip faults deforming the Cretaceous succession south of Arusan. Gr: Mesozoic granitoids, other symbols as in previous figures. (b) The eastern branch of the AFS south of Arusan, where it shows a marked transpressional character showing high-angle reverse oblique faults including several horses. (c) Schematic block diagram showing geometrical relationships among the western branch of the AFS south of Arusan shown in Figure 9A.
CP: Chah Palang Fm.; FF: Farokhi Fm.; Gr: granites; HC: conglomerates at the base of Haftoman Fm.; HF: Haftoman Fm.; Ja-Met: Jandaq Metamorphic Complex; SK: Shah Kuh; ThS: Thrust Sheet.

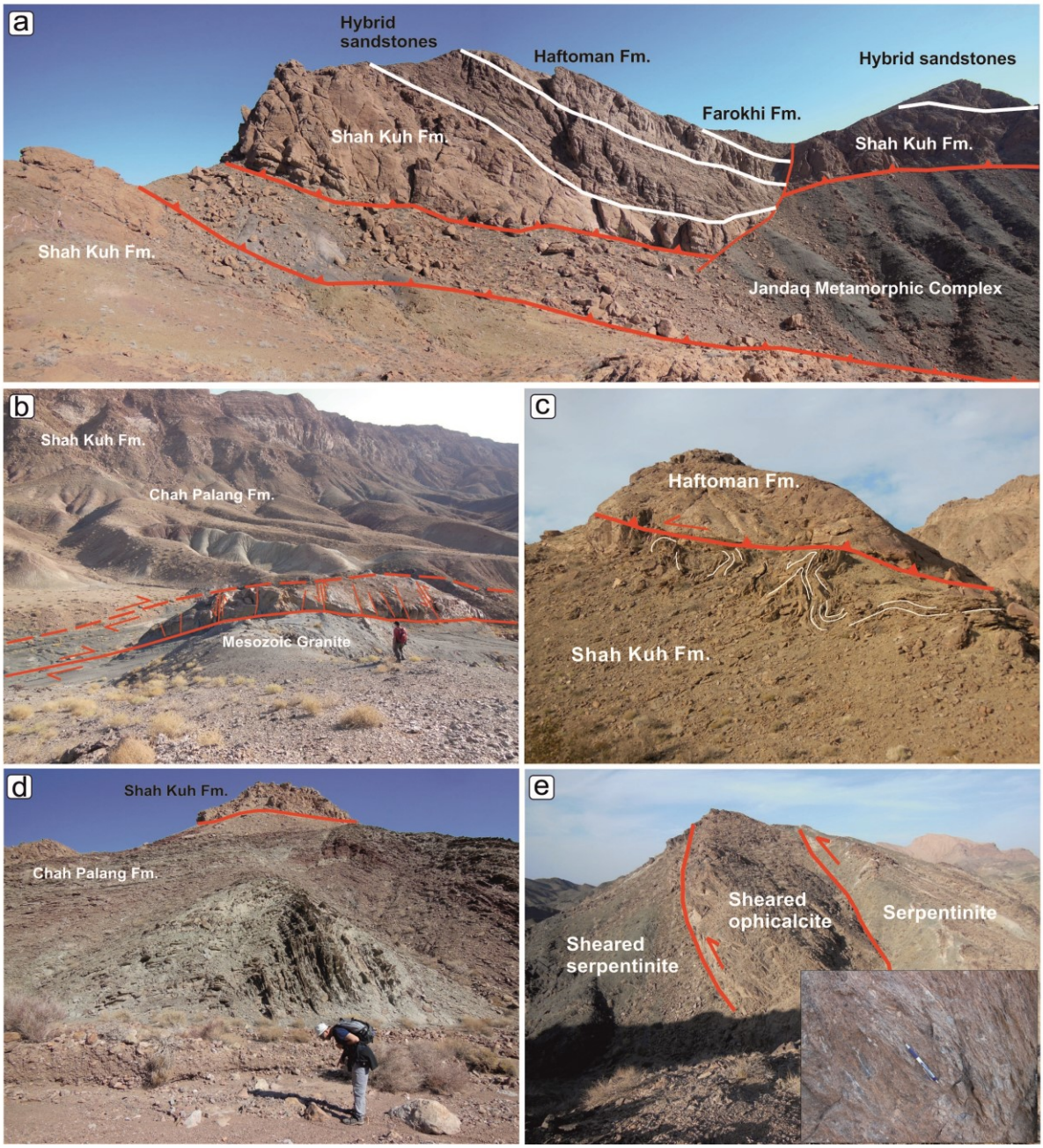

Figure 10. Field photos of the Arusan area. (a) One of the main thrusts displacing the Cretaceous successions and the metamorphic basement. Notice that the the Haftoman Formation directly cover the Shah Kuh carbonates. (b) The Western branch of the AFS at site I14-22. The fault juxtaposes Mesozoic pinki sh granitoids to the Chah Palang Formation. The Cretaceous succession is exposed on top of the Chah Palang sandstones. Secondary left-lateral faults (Riedel R1) occur between the two main dextral faults. (c) A small klippe consisting of bioclastic limestones of the Haftoman Formation overthrusting folded hybrid limestones of the Shah Kuh Formation along the western branch of the AFS at site I15-10. (d) Asymmetric closed fold in the Chah Palang sandstones along the Arusan Fault System close to the Naqi spring (Figure 3). The Shah Kuh Formation forms a klippe on top of the folded sandstones; M. Mattei for scale. (e) Sheared ophicalcite layers about 20 meters thick between imbricated ophiolites here consisting of serpentinites, NW of site I14-22 (Figure 3). The inset shows the ductile fabric developed along the shear zone within the ophicalcites.

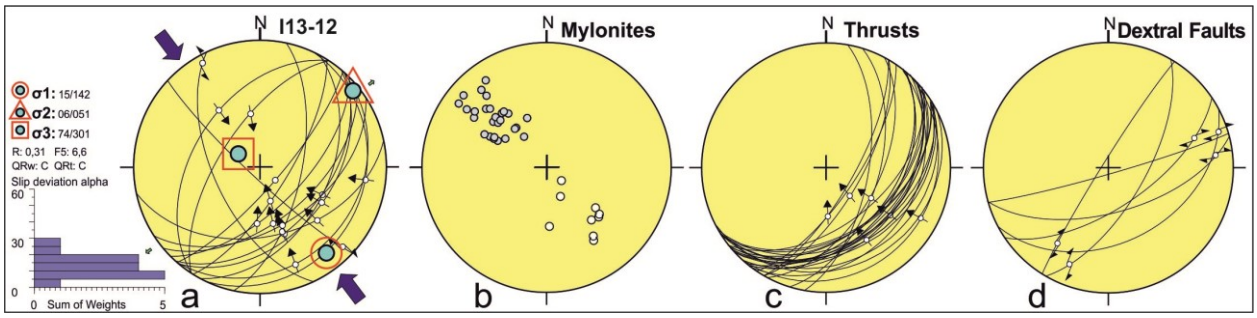

Figure 11. Mesoscopic observations within the Arusan basement consisting of ophiolites and quartzite mica schists. (a) Fault associations representing the oldest stage of NW-SE compression with faults measured within ophiolite thrust sheets. (b) Poles to mylonitc foliations (grey dots) and stretching lineation (empty dots) measured along ductile shear zone preceding the activation of faults, measured in the ophiolites. (c) The main thrust faults measured within the Arusan basement. (d) Dextral faults crosscutting thrust faults within the Arusan basement.

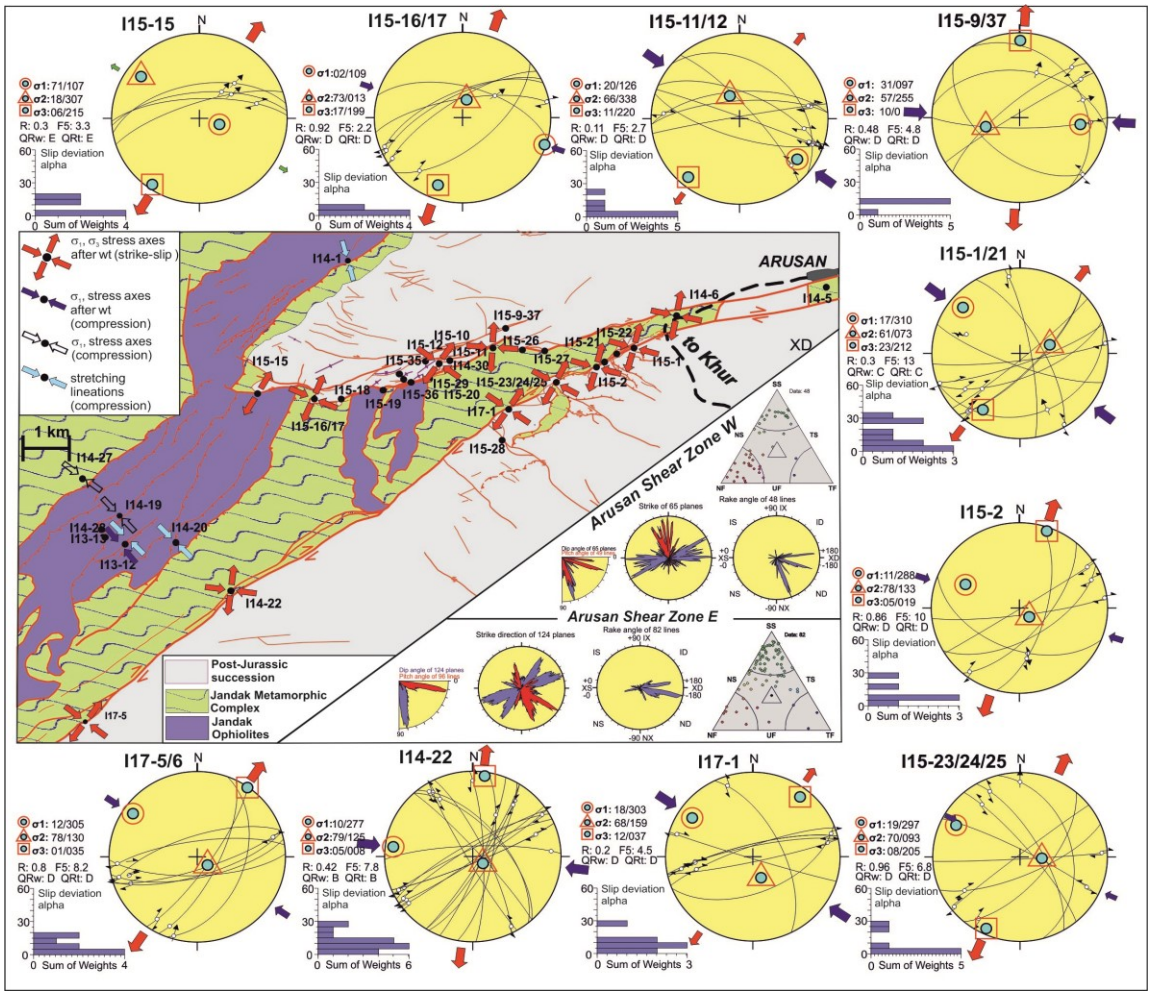

Figure 12. Paleostress reconstruction along the two main branches of the AFS. Obtained paleostress solutions are reported for each site with trend and plunge of the mains stress axes and other significant parameters, including histograms of the angular deviations alpha. See text and table 1 for additional information. Rose diagrams relative to each branch of the fault system are reported; rose diagrams represent strike (blue), dip direction (blue), dip (blue), pitch (red) and rake, with number of analysed faults. Triangular Frolich diagrams are also shown. Stereoplots, rose and Frolich diagrams were obtained with Wintensor (Delvaux & Sperner, 2013, release 5.8.9).

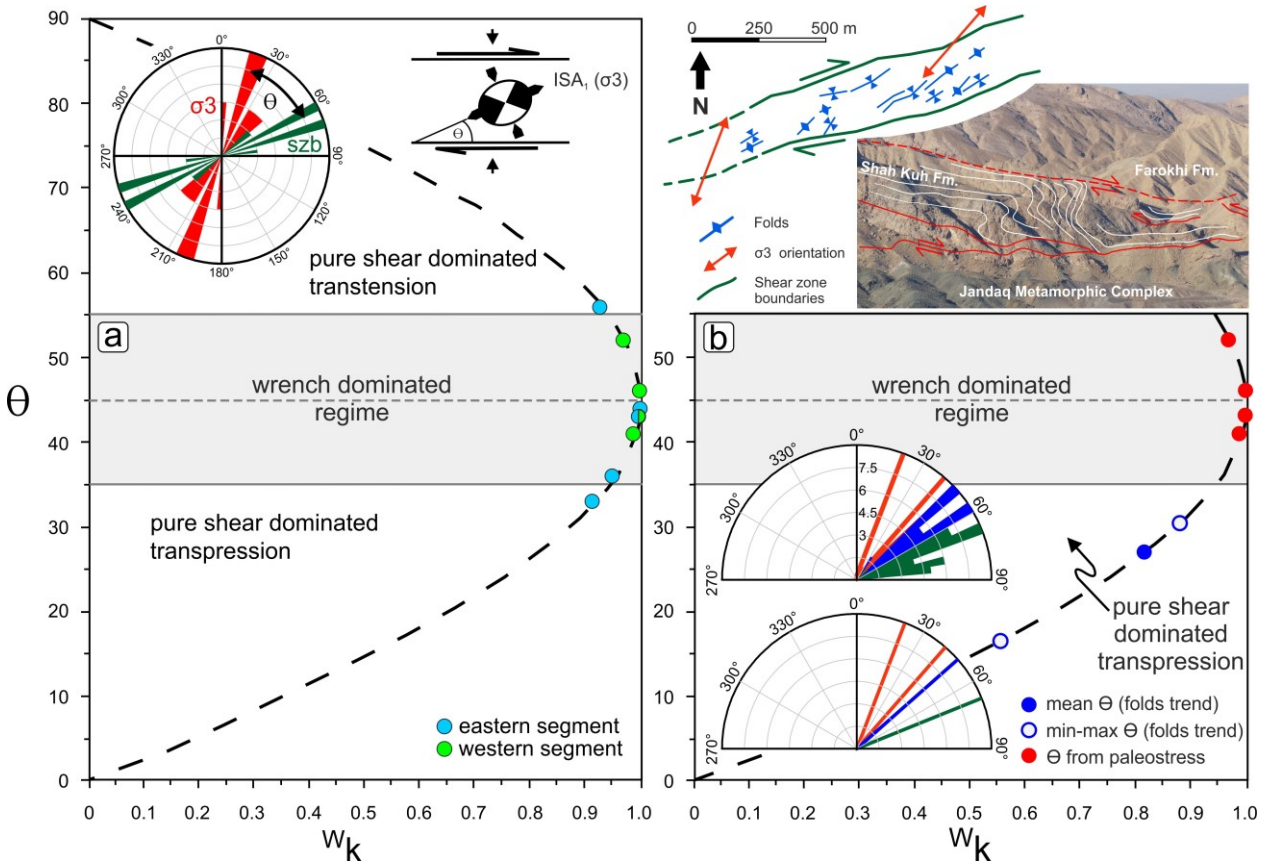

Figure 13. Relationships between the orientation of the maximum Instantaneous Stretching Axis (ISAmax) with respect to the shear zone boundary (angle θ) related to the kinematic vorticity number Wk (modified after Fossen et al. 1994; Fossen & Cavalcante, 2017). The Wk (a) has been obtained for the Arusan Western Segment shear zone (green dots) and Arusan Eastern Segment shear zone (light blue dots) and (b) for *en échelon* folds occurring in the Arusan Western Fault shear zone. In A are reported a rose diagram showing the value of θ and a schematic representation of the orientation of the ISAs. A scheme showing the shear zone boundaries, σ3 orientation and the traces of fold axial planes is also reported. szb: shear zone boundaries.

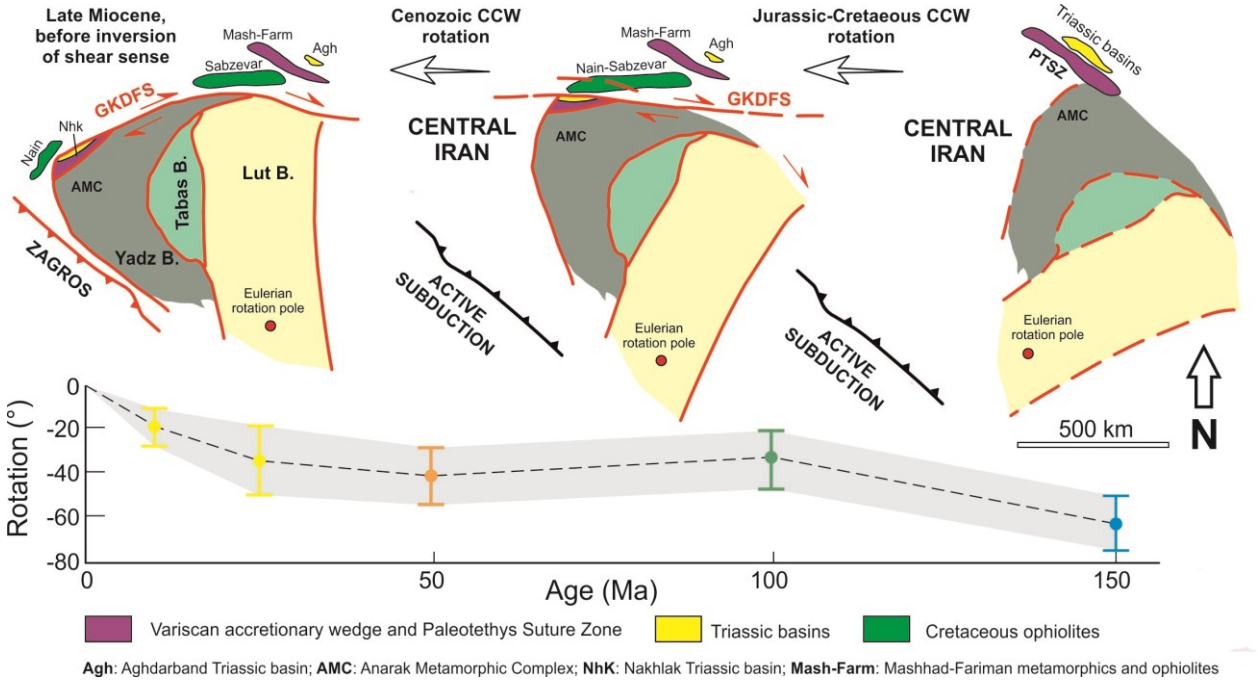

Figure 14. Two stage CCW rotation model of blocks forming the present day CEIM. A pre Late Miocene total CCW rotation (data from Mattei et al., 2015) of 65°-70° accounts for the observed displacement of the previously continuous Paleotethys Suture Zone (PTSZ) in NE Iran, as well as for the ca. 30° CCW rotation along the precursor of the GKDFS that displaced the Nain ophiolites from the Sabzevar complex. Refer to the main text for detailed description of paleomagnetic data from which rotations are inferred.

Site		Data	Used	□□□			□□□			□□□			Ratio R	Ratio R'		ANG		F5	st-dev	QRrwsm	QRt	LAT.	LONG.
				trend	plunge	□□□	trend	plunge	□□□	trend	plunge	□□□	□	□	□	(°)							
NW-verging thrust stacking																							
I13-12	**AR-OPH**	19	16	142	15	12.4	51	6	9.3	301	74	9.8	0.31	2.31		12.50	6.80	6.60	6.60	**C**	**C**	34° 05' 54"	55° 01' 49"
NE-SW dextral shearing																							
I15-15	**AWF**	4	4	98	79	19.9	318	8	27.7	227	7	23.4	0.33	0.33	E	9.00	5.40	3.30	2.20	**E**	**E**	34° 07' 02"	55° 02' 46"
I15-16/17	**AWF**	7	6	109	2	26.4	356	73	26.8	201	15	12.5	0.92	1.08	TT	3.80	2.50	2.20	3.10	**D**	**D**	34° 07' 01"	55° 03' 10"
I15-11/12	**AWF**	10	8	126	20	13.1	335	68	16.4	219	10	13.1	0.1	1.9	TP	7.10	7.20	2.60	4.10	**D**	**D**	34° 07' 17"	55° 04' 8"
I15-9/37	**AWF**	7	6	97	31	12.2	255	57	10.5	1	10	6.7	0.48	1.52	SS	10.70	5.30	4.80	2.50	**D**	**D**	34° 07' 29"	55° 04' 40"
I15-32	**MA**	4	4	137	1	18.9	46	67	29.5	227	23	28.3	0.37	1.63	SS	7.90	8.30	4.40	4.40	**E**	**E**	34° 09' 05"	55° 11' 04"
I14-6	**AEF**	4	4	101	22	20.2	311	65	32.7	196	11	34.8	0.19	1.81	TP	9.10	5.80	4.90	2.30	**E**	**E**	34° 06' 04"	55° 00' 08"
I15-1/21	**AEF**	10	10	310	17	8.6	73	61	18.8	212	23	19.7	0.3	1.7	TP	13.80	10.70	13.00	8.60	**C**	**C**	34° 07' 22"	55° 05' 24"
I15-2/22	**AEF**	7	6	288	11	30.2	133	78	30.1	19	5	8.7	0.86	1.14	TT	11.70	10.00	10.00	8.20	**D**	**D**	34° 07' 10"	55° 04' 58"
I15-23/24/25	**AEF**	11	8	297	19	49.1	93	70	53	205	8	12.4	0.96	1.04	TT	9.00	9.50	6.80	6.60	**D**	**D**	34° 07' 04"	55° 04' 55"
I17-1	**AEF**	11	8	303	18	18.9	159	68	27.1	37	12	24.7	0.2	1.8	TP	9.10	8.60	4.50	6.80	**D**	**D**	34° 06' 56"	55° 04' 34"
I14-22	**AEF**	21	16	277	10	12.1	125	79	22.3	8	5	20.7	0.42	1.58	SS	10.50	8.40	7.80	7.40	**B**	**B**	34° 05' 36"	55° 02' 35"
I17-5/6	**AEF**	10	9	305	12	3.4	130	78	14.1	35	1	14.4	0.8	1.2	TT	7.50	7.30	8.20	7.00	**D**	**D**	34° 04' 38"	55° 01' 30"
I15-4	**NSF**	18	15	93	14	9.5	184	3	13	284	75	10.9	0.18	2.18	TP	13.20	8.90	7.10	5.60	**C**	**C**	34° 03' 43"	55° 01' 38"

Table 1. Relevant information from stress inversion obtained with Wintensor software (Delvaux & Sperner, 2003). Location of analysed sites in previous figures. AR-OPH: Arusan Ophiolites AWF: Arusan Western Fault; AEF: Arus an Eastern Fault; MA: Mohammad Abad. Data: total number of measurements; Used: number of accepted faults for stress inversion; trend/plunge of the main stress axes σ_1, σ_2, and σ_3 with $\sigma_1 \geq \sigma_2 \geq \sigma_3$, with 1 sigma

standard deviation; stress ratio R $(\sigma_2-\sigma_3)/(\sigma_1-\sigma_3)$; tectonic stress regime index R' and its 1 sigma standard deviation (StDev). $R' = R$ when σ_1 is vertical (extensional stress regime), $R' = 2 - R$ when σ_2 is vertical (strike-slip stress regime), $R' = 2 + R$ when σ_3 is vertical (compressional stress regime). Quality estimator Rwsm takes into account the number of faults measurements accepted on the total number of the faults used for the inversion and the accuracy of the evaluation of the slip sense (World Stress Map project, Zoback, 1992). Quality estimator Rt also considers the heterogeneity of the fault data orientations (Delvaux & Sperner, 2003); both indexes range from A (best quality) to E (worst quality). Solutions were accepted for values of the F5 misfit function < 30 (range 0-360 from perfect fit to complete misfit) and single values of the angle $\alpha < 30°$ between the slip vector on the fault plane and the computed shear stress. F5 is an iterative function minimising the angle α, as well as the normal and shear stresses magnitudes favouring the slip on the plane.